Materials Horizons

ROYAL SOCIETY OF CHEMISTRY

REVIEW

View Article Online
View Journal | View Issue

Cite this: *Mater. Horiz.*, 2023, **10**, 3218

Ion modulation engineering toward stable lithium metal anodes

Ce Wang, Jiahao Zhu, Yuhong Jin, * Jingbing Liu, Hao Wang * and Qianqian Zhang *

Received 16th March 2023,
Accepted 10th May 2023

DOI: 10.1039/d3mh00403a

rsc.li/materials-horizons

Homogeneous ion transport during Li^+ plating/stripping plays a significant role in the stability of Li metal anodes (LMAs) and the electrochemical performance of Li metal batteries (LMBs). Controlled ion transport with uniform Li^+ distribution is expected to suppress notorious Li dendrite growth while stabilizing the susceptible solid electrolyte interfacial (SEI) film and optimizing the electrochemical stability. Here, we are committed to rendering a comprehensive study of Li^+ transport during the Li plating/stripping process related to the interactions between the Li dendrites and SEI film. Moreover, rational ion modulation strategies based on functional separators, artificial SEI films, solid-state electrolytes and structured anodes are introduced to homogenize Li^+ flux and stabilize the lithium metal surface. Finally, the current issues and potential opportunities for ion transport regulation to boost the high energy density of LMBs are described.

Wider impact

Lithium metal anodes (LMAs) have been developed for several decades due to their ultrahigh energy density and key role in energy storage and conversion. However, LMAs are unable to be applied practically due to the vulnerable solid electrolyte interphase (SEI) and uncontrolled Li dendrite growth caused by disordered ion transport during the Li plating/stripping process. Hence, homogeneous ion transport is highly desirable for high efficiency and dendrite-free Li metal batteries. To address these issues and drive the improvement of LMAs, complete understanding of the formation mechanisms of Li dendrites and SEI films and the inherent interactions is indispensable, which requires a comprehensive investigation of Li^+ transport behavior inside the battery. Here, this review renders a comprehensive study of the interactions between the Li dendrites and SEI film during Li deposition and stripping to find out the rationale of LMA performance degradation. Moreover, functional separators, artificial SEI films, solid-state electrolytes and structured anodes to homogenize Li^+ flux and stabilize the lithium metal surface are introduced. Finally, the current issues and potential opportunities for high energy-density LMAs are described. This review provides a theoretical basis for the design of high-energy LMAs that are dendrite-free for next-generation storage devices.

Key Laboratory for New Functional Materials of Ministry of Education, Faculty of Materials and Manufacturing, Beijing University of Technology, Beijing 100124, P. R. China. E-mail: jinyh@bjut.edu.cn, haowang@bjut.edu.cn, zhangqianqian@bjut.edu.cn

Ce Wang

Ce Wang received his master's degree from Beijing General Research Institute of Mining &Metallurgy under the direction of Dr Yanbin Chen in 2020. Now he is a PhD student at Beijing University of Technology under the supervision of Prof. Hao Wang. His research interests are in advanced materials for electrochemical energy storage and conversion, mainly including covalent organic frameworks and secondary battery separator materials.

Yuhong Jin

Yuhong Jin is currently an assistant professor at Beijing University of Technology (BJUT). He received his PhD from Materials Science and Technology at Beijing University of Chemical Technology (BUCT) in 2013. He then worked as a postdoctoral fellow in Prof. Xiangming He's group at Tsinghua University from 2013 to 2015. His research areas focus on the preparation and morphological design of electrode materials for lithium/sodium ion batteries, electrochemical capacitors, and fuel cells.

1. Introduction

Traditional lithium-ion batteries based on graphite anodes are barely able to meet the growing energy demand due to capacity limitations (theoretical capacity is 372 mA h g^{-1}).[1] Recently, the tremendous demand for high-energy density Li metal batteries (with LMAs as the anode) has been pursued with determination by the academic community and enterprises. LMAs have been regarded as a potential candidate for next-generation high-energy-density electrodes due to their highest specific capacity (3680 mA h g^{-1}) and lowest reduction potential (−3.04 V *vs.* standard hydrogen electrode).[2–5] Therefore, the development of stable LMAs is of great significance for solving the difficulties of energy shortage.[6]

Unfortunately, LMAs with many merits are unable to be applied practically due to the vulnerable solid electrolyte interphase (SEI) and uncontrolled Li dendrite growth during the Li plating/stripping process. The uncontrolled Li dendrite growth due to the inhomogeneous ion flux consumes a large amount of active lithium, which leads to capacity loss. And finally, it can pierce the separator causing a short circuit for a safety accident. Moreover, the fragile interface caused by the formed SEI film of an active Li metal and electrolyte also exacerbates the risk of battery degradation. Furthermore, fractured SEI films can intensify the reaction between the electrolyte and Li metal, resulting in lithium salt concentration gradients that trigger lithium dendrite growth.[7]

Excessive anion ion transport (lower Li^+ transference number t_{Li^+}) and the deficient lithium ion concentration near the Li metal anode surface are the main reasons for lithium dendrite nucleation and growth.[8] In addition, disordered Li^+ ions are deposited onto the lithium metal surface and generate unsatisfactory SEI films, which impede the transport of lithium ions and also consume a large amount of active lithium. Consequently, lithium dendrite nucleation and growth and disordered SEI film breeding are closely related to ion transport. The transport of lithium ions within the lithium battery system is a dynamic process associated with the separator, electrolyte and electrode/electrolyte interfaces.

Furthermore, severe volume changes triggered by the lithium plating/stripping process result in cracks and pits on the fragile lithium metal surface. Disordered Li^+ ion flux is preferentially deposited at defects (cracks and pits), exacerbating electrolyte depletion and dendrite growth. Conversely, proliferating dendrite growth and continuous breakage/reformation SEI film disrupts the uniform deposition of Li^+ flux. This not only increases the interfacial ion transport resistance and cell polarization but also reduces the Coulomb efficiency by separating the dendrites from the current collector and forming dead lithium. Therefore, a uniform Li^+ flux enhances interfacial stability and prevents electrolyte decomposition and excessive lithium consumption, while mitigating volume changes and dendrite growth.[9]

Several reviews have covered the mechanisms of lithium dendrites or SEI films and introduced Li^+ transport, independently.[9–16] However, limited reviews have focused on the interaction between lithium dendrites, SEI films and Li^+ ion transport during Li^+ plating/stripping. In this review, we introduce the ion homogeneity regulation that endows LMAs with uniform Li^+ flux and a stable metal surface. Firstly, the elaborated Li plating and stripping behaviors are summarized. Then, the formation mechanisms of Li dendrites and the SEI film and their effects on Li^+ ion transport are also described in detail. Thirdly, the strategies including functional separators, solid electrolytes, artificial SEI films, and structured anodes to suppress dendrites and stabilize the Li metal anode according to the ion homogeneity regulation are discussed (Fig. 1). Finally, the future perspectives and development directions of high energy density LMAs are prospected.

2. Li plating/stripping behaviors

Lithium plating and stripping is the most important electrochemical process for lithium batteries, which directly affects the development of high energy storage devices. Moreover, the

Hao Wang

Hao Wang is a professor at the faculty of materials and manufacturing, Beijing University of Technology, China. Prof. Wang received his PhD in applied chemistry in 1997 from Beijing Institute of Technology, China. Then he worked as a postdoctoral fellow at Tokyo Institute of Technology, Japan. His current research interests are focused on advanced materials for electrochemical energy storage, and electrochromic materials and devices.

Qianqian Zhang

Qianqian Zhang is currently a professor at Beijing University of Technology (BJUT). She received her PhD in materials physics and chemistry from Beihang University in 2015 (Jin Zhai's group), and then worked as a postdoctoral fellow in Prof. Xungang Diao's group at Beihang University. Her current scientific interests are focused on the design and fabrication of nanofluidic membranes for boosting electrochemical ionic devices including electrochemical cells and electrochromic devices.

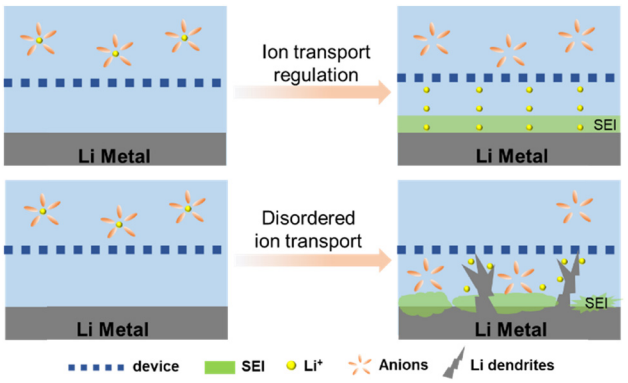

Fig. 1 Schematic diagram of the suppression of Li dendrite growth by ion transport.

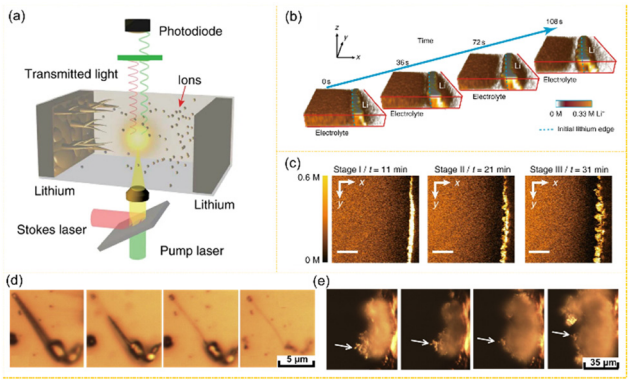

Fig. 2 *In situ* characterization of the lithium deposition process. (a) Schematic illustration of the experimental design. (b) Visualization images of lithium dynamic deposition. (c) The three-stage lithium deposition process. Reproduced with permission from ref. 20. Copyright 2018, Nature. (d) The dissolution process of lithium dendrites. Reproduced with permission from ref. 23. Copyright 2014, Elsevier. (e) The bush-like Li stripping and subsequent electroplating process. Reproduced with permission from ref. 8. Copyright 2014, Elsevier.

notorious lithium dendrites and unstable SEI film are also closely associated with the Li plating/stripping process.[17] Investigating the dynamic electrochemical process by operando characterization is beneficial for researchers to have a better understanding of Li^+ flux dynamics and guide the design of high-efficiency LMAs.[18]

Li plating is a dynamic process of Li^+ in the electrolyte, which needs operando characterization technology to explore the potential mechanisms.[19] Bazant *et al*. investigated the morphology of lithium deposition using capillary cells and found the transformation from the mossy Li to the Li dendrites.[8] Yang and co-workers further elucidated the dendrites transformation process by *in situ* stimulated Raman scattering (SRS) microscopy (Fig. 2a).[20] Fig. 2b shows that the lithium-ion concentration near the lithium metal surface decreased until fully depleted as the lithium deposition depth increased. It is noteworthy that the deposition morphology of lithium has also gradually changed. As shown in Fig. 2c, in the initial stage (stage I), the lithium-ion concentration is not depleted and mossy Li is slowly generated; then, the lithium-ion concentration is partially depleted. It can be observed that the mossy Li and dendrites grow together (stage II); finally, dendrites dominate growth after the lithium-ion concentration is full depleted (stage III). Moreover, lithium salt concentration and Li^+ surface migration also play an important role in the Li plating morphological evolution.[19,21,22] Thus, dendrite morphology growth is expected to be mitigated by regulating the lithium-ion concentration and transport according to the deposition mechanism.[21,22]

The limited understanding of Li stripping behavior is also an obstacle to obtaining stable LMAs with a long cycle life due to the complicated transient reaction. Fig. 2d and e show the different dissolution behaviors of Li dendrites and mossy Li by using *in situ* microscopy, respectively. As shown in Fig. 2d, the needle-like Li starts to dissolve from the tip instead of shrinking the whole structure due to the SEI film holding the Li dendrites structure.[23] This suggests that the structure and compositions of the SEI film have a critical effect on the dissolution of dendritic lithium. An inhomogeneous component or broken SEI film will affect the dissolution of Li dendrites, threatening the safety performance of LMAs.[24] Unlike Li dendrites, Li mossy exhibits a completely different dissolution mechanism. Lithium mossy simultaneously dissolves starting from the bottom, while the top structure remains unchanged (Fig. 2e). Moreover, the top structure of Li mossy likely evolves into lithium dendrites.[8]

The dendritic lithium dissolves and still leaves an empty shell in the SEI film and the mossy Li may cause electrical insulation from the substrate due to the bottom-up dissolution mechanism. The repeated generation of SEI shells not only affects the mechanical integrity of the SEI film but also accelerates the decomposition of the electrolyte. The remaining lithium is insulated with the substrate to form the dead lithium, which is the main source of battery performance degradation.[24]

3. Issues from disordered ion transport on the LMAs

Unstable solid electrolyte interphase (SEI) films and notorious lithium dendrites are two fatal defects that hinder the development and commercialization of LMAs. Therefore, it is necessary to investigate in depth the formation mechanism of these defects and the effect on the transport of Li^+. Moreover, the interaction of SEI films and Li dendrites also plays an important role in high-performance LMAs.

3.1 Unstable solid electrolyte interphase (SEI) films

The thin film formed between the anode and electrolyte interface is called the solid electrolyte interphase (SEI), and it plays a key role in protecting the electrolyte solution from reaction with Li metal anodes. Despite the tremendous efforts of scientists to gain a deeper understanding of SEI, the mechanism of SEI formation, components and structure still remains

ambiguous.[25–37] Hence, the overall summary of the formation evolution mechanism, compositions and structure model of SEI is essential for us to explore the potential interactions between SEI properties and LMA performance.[9–11]

3.1.1 The formation mechanisms of SEI. The formation of SEI film is complicated and closely related to the molecular orbital of the electrolytes and the cathode and anode electrodes.[38] The lowest unoccupied molecular orbital (LUMO) and highest occupied molecular orbital (HOMO) of electrolytes and the electrode are illustrated in Fig. 3a. The energy gap of the electrochemical potentials of electrodes (μ_C represents cathode and μ_A represents anode) and molecular orbital energy (E_{LUMO} and E_{HOMO}) govern the formation of interfacial films. Generally, if E_{LUMO} is lower than μ_A, the electrons will incline to transfer from the anode to electrolyte, and the electrolyte is reduced. Likewise, if E_{HOMO} is higher than μ_C, the electrolyte will donate electrons and be oxidized.[9,39] Moreover, only when the interphase is thermodynamically stable internally, can the cells operate safely.[40]

3.1.2 The formation process of SEI. SEI is mainly composed of the decomposition products of electrolytes and the formation can consist of several steps: unavoidable lithium passivation, chemical reaction and electrochemical reaction (Fig. 3b). Practically, untreated Li metal will inevitably react with traces of air to form oxides on the surface due to its high chemical activity nature.[41] Moreover, the Li metal will spontaneously and quickly react with the electrolyte solution due to the high chemical activity, forming the primitive SEI film with insoluble products.[42] Subsequently, SEI thickening is triggered by the continuous electrochemical reaction of salt and solvent molecules.[43] The SEI film growth is accompanied by the participation of electrons/electrolytes.[44,45]

Except for the electrochemical reaction between Li metal with electrolyte solution, the electric double layer (EDL) at the interface also has an important effect on the formation and growth of the SEI film.[46–48] EDL is generated by the accumulation of charge excesses occurring on the electrode/electrolyte solution, and the driving forces are Coulombic forces and chemical interactions at the electrode surface. The negatively charged surface of the lithium metal will contribute to a large cation enrichment and anion deficiency in the EDL. Moreover, the EDL can change the reduction voltage of SEI films, and modulate the Li^+ coordination clusters and the reduction potential of free electrolyte species, thus affecting the growth process of SEI membranes.[49] Moreover, the formation time of EDL is extremely short ($\sim 10^{-8}$ s), and is much less than the time of redox reactions ($\sim 10^{-4}$–10^{-2} s), indicating that EDL formation precedes SEI.[50] Furthermore, the EDL consists mainly of ions (anion-predominant) and molecules that have strong interactions with the electrode surface, and the charge rearrangement and accumulation occur at the interface. The formation of SEI is a complex behavior and the chemical and physical reactions of the different components at the electrode/electrolyte interface should be considered comprehensively.

3.1.3 The structure model of SEI. Due to the important role of SEI film for battery performance, the exploration of structure models has been pursued. However, the environmental sensitivity of SEI and irreversible structural damage from analytical tools pose a great challenge to studying the structural components and distribution of SEI. In addition, the structure and components of the SEI may change under light, electron, magnetism, X-ray and neutron-based characterizations, thus presenting a false structural model or interpretation. Fortunately, after decades of arduous efforts, understanding of the SEI structure has been improved and various models such as a single crystal model, mosaic model, multilayer model and dual-layer structure have been proposed.[25,36,51,52]

Generally, the current widely accepted models are the mosaic model and dual-layer structure. As shown in Fig. 3c, the mosaic model has an uneven surface, which consists of reductive decomposition products (inorganic-rich layer and organic-rich layer) inlaid with each other. Moreover, investigating the structure of SEI using the mosaic model is highly compatible with the results of XPS and the component order of the SEI film.[53] Furthermore, the dual-layer model further elucidates the SEI component arrangement. Fig. 3d displays the typical dual-layer model. The inner layer consists of inorganic material (Li_2O, Li_3N, LiF, LiOH, Li_2CO_3), and the outer layer mainly includes organic species such as $ROCO_2Li$, ROLi, and $RCOO_2Li$ (R is related to the organic group).[54] Overall, the SEI film is composed of the inorganic inner layer and organic outer layer, and the species are cross-linked with each other without clear demarcation lines.

3.1.4 Compositions of SEI. Chemical components are essential for SEI films and are highly related to electrolyte and ion diffusion.[55,56] In this section, the commonly inner inorganic SEI components (LiF, Li_2O, Li_3N or LiN*x*O*y*, LiH and Li_2CO_3) and the outer organic layer ($ROCO_2Li$ and $(ROCO_2Li)_2$) under conventional electrolytes are discussed. As shown in Table 1, the energy barriers of Li^+ diffusion and the band gap of several inorganic SEI components are summarized.

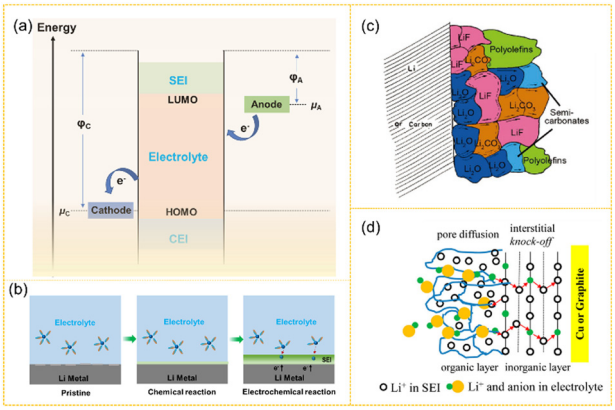

Fig. 3 (a) Schematic of the formation theory of an electrode/electrolyte interphase film. (b) Schematic illustration of the formation process of SEI. Scheme of SEI models. (c) The mosaic model in the top view. Reproduced with permission from ref. 51. Copyright 1997, Electrochemical soc inc. (d) The dual-layer model in the cross-section view. Reproduced with permission from ref. 36. Copyright 2012, American Chemical Society.

Moreover, from the physical properties of components, we can initially identify which components are positive or detrimental to SEI stability.

LiF is a fascinating SEI species generated by the reduction of F-containing electrolytes, which plays a positive role in SEI stability. Theoretically, LiF has a high energy barrier of Li^+ diffusion (0.729 eV) and band gap (8.9 eV), which may limit the transport of lithium ions.[65] However, LiF can exhibit high surface energy and low diffusion barriers when interacting with other substances (Li_2O, Li_2CO_3) on the nano-scale level, thus improving the ionic conductivity and promoting uniform deposition of lithium ions.[66,67] Yao and co-workers proposed porous lithium fluoride (LiF) to suppress the Li dendrites and achieved long cycling under a high current density (4 mA cm^{-2}).[68] Li_2O originates from the passivation layer of Li metal and may be consumed with electrochemical cycles to contribute active lithium.[62,69] The energy barrier of Li^+ diffusion and the band gap of Li_2O are 0.152 and 4.7 eV, respectively. Furthermore, the high surface energy and the low migration energy are kinetically unfavorable for dendrite growth. Hence, Li_2O is often used to stabilize the Li metal anode to facilitate ion transport.[61] Li_3N (or LiN_xO_y) with good wettability to Li is the reduction product of $LiNO_3$ in the electrolyte, and the low energy barriers of Li^+ diffusion and band gap give it excellent Li^+ conductivity.[70] Moreover, Li_3N (or LiN_xO_y) displays a high overpotential compared with electrochemical cycle processes. Hence, it has the potential to suppress dendrites.[71]

LiH is a controversial component regarding whether it is present in the SEI fraction.[72–74] Until recently, Hu and co-workers used synchrotron-based X-ray diffraction (XRD), pair distribution function (PDF) analysis and density functional theory (DFT) calculations to identify the LiH and confirmed an active role in the SEI membrane.[75] However, LiH is considered a harmful component due to the consumption of lithium and the poor electrical conductivity and brittle nature.[76–78] Li_2CO_3 is a common compound that is formed by the reaction of active lithium metal with traces of air and electrolyte. The band gap and energy barriers of Li^+ diffusion of Li_2CO_3 are 5.0 and 0.77 eV, respectively, which indicates that Li_2CO_3 is extremely detrimental to the transport of Li^+ ions.[64] Moreover, although the Li/Li_2CO_3 interface is more stable, it is still easy to trigger dendrite nucleation and growth due to the lower electron tunneling barrier compared with the Li/LiF interface.[79,80] Furthermore, the high diffusion barrier and low surface energy of Li_2CO_3 are preferable giving rise to dendrite morphology.[39,60] Consequently, purely Li_2CO_3 is an undesirable component for SEI films to obtain dendrite-free high-performance LMAs.

In summary, the various SEI components are not independent of each other, but rather synergistically affect the SEI film and the LMAs.

3.1.5 Ion transport through SEI film. As an essential pathway for ion diffusion, the transport mechanism of Li^+ through the SEI film plays an important role in the performance of LMAs. The diffusion of Li^+ near the SEI film consists of two main parts, desolvation and crossing the SEI film.[81,82]

Desolvation of Li^+ ions. Theoretically, only naked Li^+ ions can obtain electrons and are reduced on the current coll. Therefore, the solvated lithium ions should first shed solvent molecules before the Li^+ ions deposit.[83,84] The solvation structure of Li^+ is closely related to the lithium salt concentration and solvent species, which influence the desolvation activation energy.[85–89] Ogumi and co-workers investigated the desolvation behavior of Li^+ using electrochemical impedance spectroscopy and found that the transfer activation energy of solvated Li^+ was more than twice that of naked Li^+, suggesting that desolvation of Li^+ was a critical process for Li^+ transfer kinetics.[90] This idea has also been reported in other literature reports.[82,91] Hence, enhancing the desolvation of Li^+ in the electrolyte solution can promote the Li^+ diffusion kinetics thus improving the rate performance of batteries.

Li^+ ions cross the SEI film. Fast Li^+ transport of SEI film is essential for LMAs with dendrite-free Li morphology. It is worth exploring the potential contacts between the Li^+ transport mechanism in the SEI film and SEI components and structure, which can guide the design of safe LMAs. According to solid-state ion conduction, defects can facilitate ion conduction, so Li^+ is often transported *via* grain boundaries or interstitials and vacancies.[28,92,93] In addition, the main inorganic components of SEI film, LiF, Li_2O and Li_2CO_3 also influence the Li^+ transport in SEI film. These are all insulated according to the band gap, and the high energy barriers of Li^+ diffusion limit the Li^+ diffusion.[53,94] However, when the LiF/Li_2O and LiF/Li_2CO_3 grain boundaries exist, SEI not only promotes Li^+ transport but also suppresses the decomposition of the electrolyte.[91,95] The synergistic effect of three main inorganic components in a complex chemical environment affects ion transport.

In general, the formation of SEI film is accompanied by complicated chemical and electrochemical reactions, and its components and structure are closely related to ion diffusion. Therefore, it is expected to obtain dense, continuous and impermeable SEI film by regulating ion transport to boost LMAs.

Table 1 The physical properties of SEI compositions

Compositions	Energy barriers of Li^+ diffusion (eV)	Band gap (eV)	Surface energy (eV)	Diffusion barriers (eV)	Ref.
LiF	0.729	8.9	~1.93	~0.16	57–60
Li_2O	0.152	4.7	~3.3	~0.26	60–62
Li_3N or LiN_xO_y	0.007–0.038	1.1			60 and 63
LiH					
Li_2CO_3	0.77	5.0	~0.85	~0.24	60 and 64
Organics	—	—			

3.2 Deleterious dendritic growth of Li

Metal dendrite deposition is a universal phenomenon, which is widely present in Ni, Cu, Zn, Ag and Sn.[96,97] The dendrite phenomenon of metals (such as Ni, Cu, Zn, Ag, and Sn) is investigated and the formation mechanism has been comprehensively understood, which does not affect its practical application.[97] However, Li^+ plating/stripping repeatedly in Li metal batteries is complicated, which requires a thorough understanding of the Li dendrite formation mechanism and critical influence factors to eliminate Li dendrites. In this section, we introduce the main Li dendrite-inducing factors including the ion concentration gradient and current density.

3.2.1 Ion concentration gradient. Li dendrite deposition is a dynamic electrochemical process and many scholars have built models to simulate Li dendrite nucleation and growth.[98] Recently, several insightful and referential models with simplified electrodes and electrolytes have been proposed to explore the formation mechanisms of Li dendrites.[99] For example, the heterogeneous nucleation model[100] (in which Li^+ is heterogeneous with the substrate), surface nucleating and diffusion model[101] (emphasizing the surface migration energy of Li^+), space-charge model[96] (associated with the Li^+ concentration gradient), and SEI-induced nucleating model[102] (related to the structural uniformity, diffusion coefficient and mechanical strength of SEI film). Overall, the formation of Li dendrites is associated with inherent cell system properties (substrate and SEI film, *et al.*). Moreover, the Li^+ concentration gradient plays an important role in Li depositions and can be regulated to alleviate the Li dendrites. Hence, the Li^+ concentration gradient needs to be further investigated to elucidate the ion concentration changes during Li^+ plating/stripping.

The steady state of the electrolyte without an ionic concentration gradient will be destroyed when the Li ions diffuse during the electrochemical cycling process. During the Li^+ deposition on the electrode, partially active lithium will be consumed by the SEI film causing an ion concentration gradient. Thus, inhomogeneous ion concentration distribution near the electrode affects the Li^+ deposition morphology. Moreover, the anion concentration of the electrode surface decreases during Li^+ diffusion and generates a space charge and an electric field, which causes dendrite generation.[103] Therefore, regulating ion transport (promoting Li^+ conductivity or immobilizing anions) can suppress the Li dendrites induced by the space charge.[39]

According to the effective diffusion equation, the salt concentration near the surface of the electrode decreases to zero at a Sand time (t_{sand}) when exceeding the diffusion limit.[104–107] In addition, this will disturb the uniform electroplating and induce the preferential deposition of depleted cations on the surface protrusions, leading to dendrite growth.[108,109] To alleviate Li dendrite growth, we need to extend the Sand's time according to the Sand's formula:

$$t_{sand} = \pi D_{app} \frac{(z_c c_0 F)^2}{4(J t_a)^2} \quad (1)$$

where z_c represents the charge number of the Li^+, c_0 represents the bulk salt concentration, F is Faraday's constant, J is the current density and t_a represents the anion transference number, $t_a = 1 - t_{Li}$, where t_{Li} is the Li^+ transference number.

Hence, decreasing the anion transference number (enhancing the Li^+ transference number) can delay the time for the Li^+ concentration to decrease to zero, thus inhibiting dendrite growth.

3.2.2 Current density. Except for the ion concentration gradient, the current density also plays an important role in Li dendrite growth.[110] Generally, some reports show that the Sand's time is inversely proportional to the primary (or quadratic) current density, indicating that a low current density facilitates the achievement of dendrite-free.[106,111] Sand's formula also verifies this point. Moreover, Newman and coworkers further demonstrated that the dendrite tip growth rate is directly proportional to the current density.[110] Overall, the low current density suppresses the Li dendrites growth and facilitates stable battery operation. It is noteworthy that even at low current densities, a small number of dendrites still exist due to local interface inhomogeneities.[112,113]

Overall, unstable SEI film and Li dendrite caused by disordered ion transport are the main factors hindering the development of high-performance LMAs. Conversely, the SEI film (formation, components, properties) and Li dendrite (nucleation, growth) also affect the homogeneous diffusion of Li^+ and exacerbate performance degradation (Fig. 4). Hence, uniform SEI film and inhibited Li dendrite growth can be obtained by regulating ion transport, which enhances the surface stability of LMAs and facilitates their commercialization.[114–117]

4. Strategies of homogeneous Li^+ flux for stabilising LMAs

Blocking the dendrites growth and strengthening the SEI film stability through homogeneous ion transport regulation is an effective strategy to enhance the electrochemical performance of LMAs. Functional separators, artificial SEI film, solid electrolyte and structured anode can homogenize the Li^+ ion flux and thus achieve a dendrite-free lithium metal anode (Fig. 5).

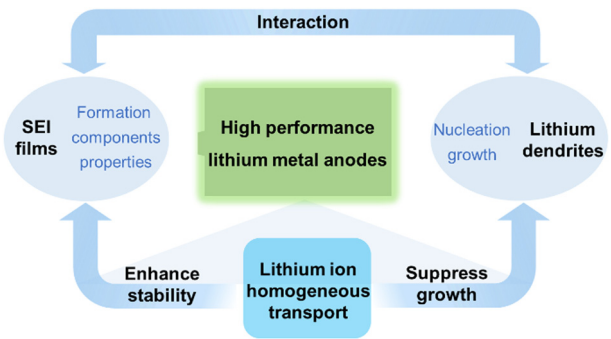

Fig. 4 Ion homogeneous transport inhibits Li dendrite growth and enhances SEI film stability.

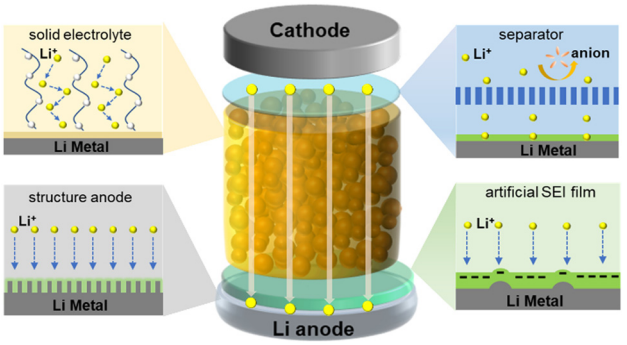

Fig. 5 Strategies for the suppression of Li dendrite growth by ion transport.

4.1 Constructing functional separators

Separators act as separate layers to prevent a short circuit caused by direct contact between the cathode and anode and grant the ions transport. High physical and chemical stability and ion conductivity are the most basic requirements for primary separators. However, commercial separators with poor wettability and permeability electrolytes cannot meet the requirements of complicated LMAs, which are plagued by lithium dendrite problems due to disordered ion transport.[118] In order to drive the development of LMAs, constructing functional separators with ion uniform transport is the preferential strategy to alleviate dendrite nucleation and modulate SEI films.[119]

4.1.1 Lithiophilic sites. Lithiophilicity refers to the affinity between Li species and a host substrate, and was firstly proposed by Cui's group.[120] It can affect the nucleation overpotential of Li^+ plating. Moreover, the large nucleation overpotential represents the thermodynamic mismatch between Li and the substrate, which results in a concentrated distribution of ions and the dendrite nucleation and growth. Therefore, functional separator anchored lithiophilic sites can decrease the overpotential to effectively homogenize Li^+ flux and guide Li nucleation, thus suppressing dendrite growth.

The Li nucleation overpotential of different metal substrates was investigated by Cui *et al.*, Mg, Zn, Ag and Au substrates exhibit almost no nucleation overpotential and ultralow nucleation barriers.[121] Hence, these metals are always used to regulate Li^+ uniform nucleation as lithiophilic sites. Song[122] reported a separator engineered by single-side deposition of magnesium (Mg) nanoparticles to induce uniform deposition of lithium metal and change the deposition direction of lithium (Fig. 6a). The heterogeneous nucleation sites (Mg nanoparticles) with a guiding effect served Li crystal seeds and reduced the nucleation overpotential in the early plating stage, resulting in stable lithium deposition stripping behavior and excellent electrochemical properties (Fig. 6b–d). In addition, the interfacial impedance and CE of batteries were alleviated due to the high chemical and mechanical stability of Mg sites.

In addition to the affinity between metals and lithium, lithiation sites can also direct the diffusion of lithium ions, which in turn affects the deposition and stripping of lithium. Sun and co-workers constructed ion selective separators with continuous lithiation sites ($-SO_3Li$) that can effectively facilitate lithium in transport. As shown in Fig. 6e, the aligned $-SO_3Li$ sites offered hopping pathways for Li^+ ion transport, which greatly reduced the ion transport barriers.[123] The $-SO_3Li$ sites not only promoted the rapid Li^+ transport but also inhibited the anion diffusion, thus enhancing the Li^+ transference number (Fig. 6f) and suppressing the Li dendrites growth. Li–S batteries with a functional separator decorated by lithiation sites exhibited excellent capacity retention (Fig. 6g). This strategy highlights the importance of the lithiophilic sites in LMAs.

4.1.2 Nanochannels. The regulation of ion-selective transport is significant for the inhibition of lithium dendrite growth caused by excessive anion transport. Nanochannels are widely present in biological systems and artificial materials, which play a critical role in ion transport.[124–126] The tunable nanoscale aperture and excess charge on the interior surface of nanochannels can suppress anion diffusion and promote Li^+ transport thus alleviating dendrite growth. Moreover, the physical and chemical properties of nanochannels, such as size shape, wettability, charge and other interactions will affect ion transport. For example, tuning the size of nanochannels can sieve ions according to the difference in radius (size confinement). Excellent wettability facilitates the diffusion of the rapid ions and can be improved by decreasing the pore size. The electrostatic interactions between charges and ions have an important role in the ion transport process. Hence, constructing separators with nanochannels can promote Li^+ transport and inhibit anion diffusion, thus suppressing dendrite growth and enhancing electrochemical performance.

Kim and co-workers[127] synthesized a track-etched polyimide (TEPI) separator with nanochannels decorated with polyvinylpyrrolidone (PVP), as shown in Fig. 7a. A uniform Li^+ transfer and Li_3N-rich SEI film were obtained *via* the rigid nanochannels. Moreover, the stable Li plating/stripping process was enhanced. The wettability and ionic conductivity were also improved due to the abundant pores (Fig. 7b and c). However, the large pore size (average of 100 nm) limited the ion selectivity and long-cycle stability. Lu and co-workers[128] fabricated a separator containing nanoscale micropores with a metal–organic–framework (MOF) and poly(vinyl alcohol) by an electrospinning process, and the ion channels of MOFs spontaneously blocked anions while facilitating Li^+ transport (Fig. 7d and e). Moreover, LiF-rich SEI films were generated and promoted the cycling stability of the batteries, which was ascribed to the ion selectivity achieved by MOF channels (Fig. 7f). Although these functional separators with nanochannels can modulate ion transport and SEI film components, the large pore size or non-uniform dense nanochannels are dissatisfied for LMAs.[129]

4.1.3 Polar groups. Extensive literature has demonstrated that the separator with polar groups can redistribute the Li^+ ion flux and enhance the homogenous Li plating.[130,131] Wu and co-workers[132] prepared functional separators with 2D molecular brushes (polyacrylamide-grafted graphene oxide nanosheets,

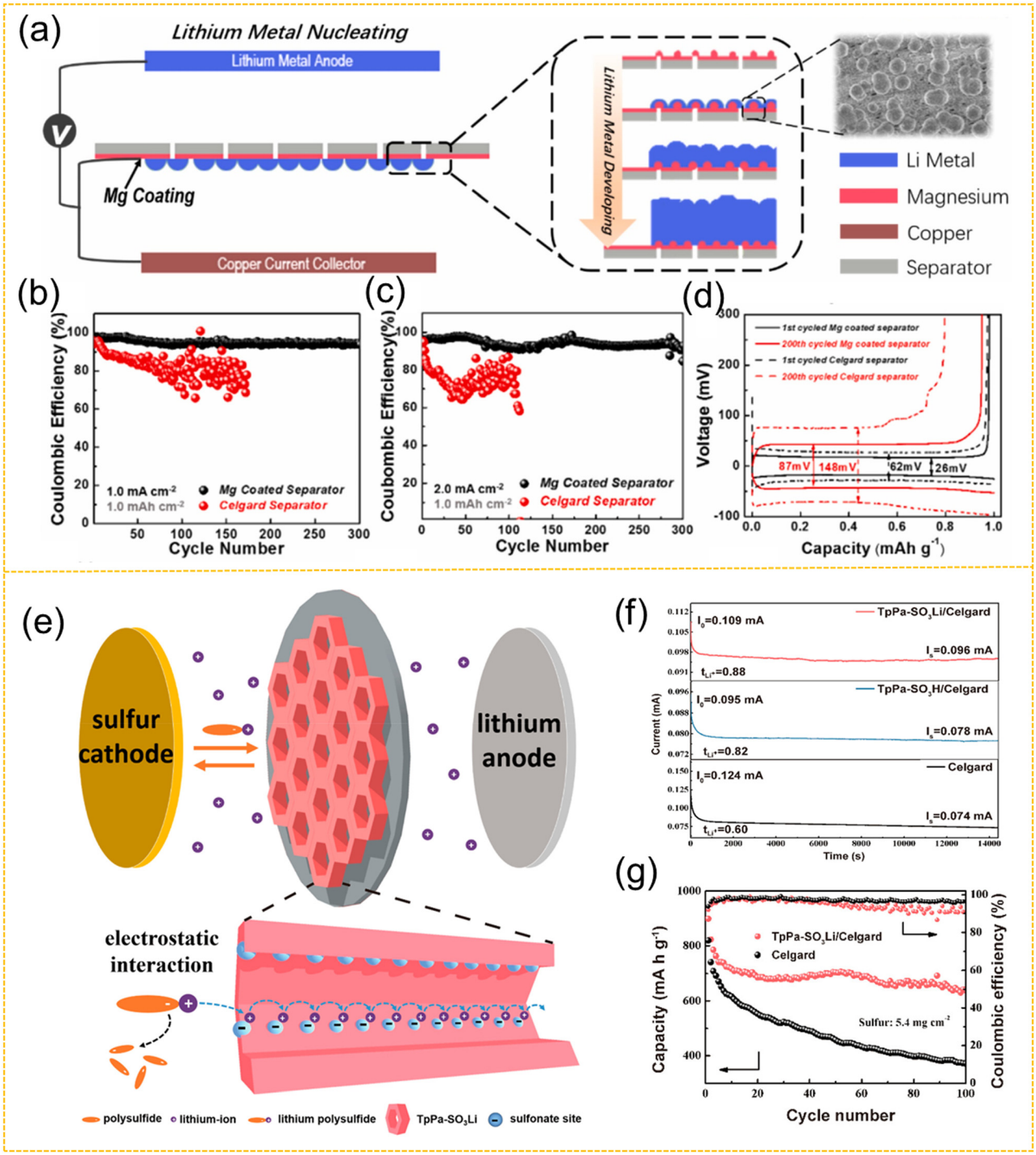

Fig. 6 The functional separator with lithiophilic sites. (a) A schematic illustration of electrodeposition with a Mg-coated separator. (b–d) Li^+ ion depositional/stripping behavior of Li//Cu cells. Reproduced with permission from ref. 122. Copyright 2019, Elsevier. (e) A scheme of the separator with sulfonate sites. (f) *I*–*t* curves of Li//Li symmetric batteries. (g) Cycling performance of Li–S batteries with a high sulfur loading of 5.4 mg cm^{-2}. Reproduced with permission from ref. 123. Copyright 2021, American Chemical Society.

GO-*g*-PAM) by simply blade-coating to obtain a uniform Li deposition and dense SEI film (Fig. 8a). The polar groups (C═O and N–H bonds) of hairy PAM chains on the GO surface provided separators with abundant active sites for effective attachment and uniform distribution of Li ions at the molecular level. Moreover, the interconnected interspaces between the stacked 2D molecular brushes provided a fast pathway for electrolyte diffusion. The functional separator exhibited excellent cycling stability (1900 h) even at ultra-high current densities of 20 mA cm^{-2} (Fig. 8b and c).

In addition to homogenizing Li^+ flux, polar groups (*e.g.*, the carboxyl group) also play an important role in forcing the

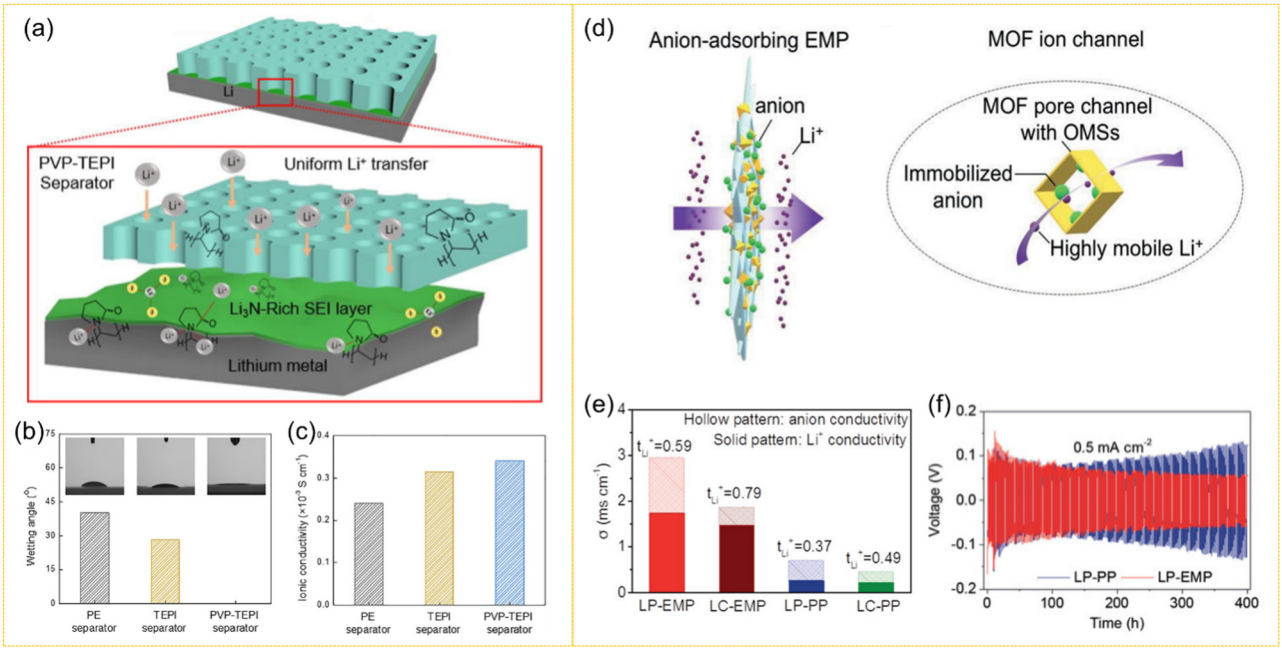

Fig. 7 A functional separator with nanochannels. (a) Schematic of the PVP–TEPI separator with rigid nanochannels. The wettability (b) and ionic conductivity (c) of separators. Reproduced with permission from ref. 127. Copyright 2022, Elsevier. (d) Schematics of the MOF-based (EMP) separator with pore channels for regulating ion transport. (e) The Li^+ transference number and ion conductivity of separators. (f) The cycling performance of Li//Li symmetrical batteries with different separators. Reproduced with permission from ref. 128. Copyright 2019, Wiley.

breakage of the fluorinated bond in the electrolyte.[133] Moreover, these groups can regulate electrolyte degradation and control the chemical environment inside the batteries. Tao and co-workers[134] developed self-assembled monolayers (SAMs) with high-density and long-range-ordered polar carboxyl groups linked to an aluminum oxide (AAO)-coated separator to affect the electron transfer kinetics and alter the electrochemical redox kinetics of the electrolyte, thus modulating the nanostructure of the SEI. As shown in Fig. 8d, the carboxyl group devoted excess electrons to accelerate the decomposition of the C–F bond of LiTFSI (Fig. 8e), which promoted the generation of LiF-rich SEI films confirmed by Cryo-TEM (Fig. 8g) and stabilized the Li/electrolyte interface. Consequently, the SAMs with carboxyl groups substantially inhibited the formation of Li dendrites and extended the lifetime of Li anodes (Fig. 8f).

4.1.4 Desolvation interfaces. Generally, the solventized lithium metal ions are accompanied by a typical desolvation process during the discharge/charge process. Moreover, the desolvation of Li^+ generates a lot of highly reactive solvent molecules, causing instability at the electrode/electrolyte interface during Li^+ plating/stripping.[135] Furthermore, this process usually occurs in the electrode/electrolyte interphase and has a significant impact on the composition and morphology of the SEI film and the ionic conductivity.[136] Therefore, to overcome the inherent defects in Li^+ disinsertion and insertion, the desolvation process of lithium ions can be advanced from the highly reactive interface to the nanochannel of the functional separator.

The functional separator with the physicochemical interaction can remove the free solvent molecules to obtain a high Li^+ concentration to delay the Sand's time after desolvation. Liu and co-workers[137] synthesized the TPB-BD$(OH)_2$-COF separator with abundant hydroxyl functional groups (–OH) which could form hydrogen bonds (–OH···F and –OH···O) with dilute electrolytes (Fig. 9a–d). The abundance of free molecules in the solvent sheath was reduced to obtain desolvated Li^+ ions. Moreover, a high-strength LiF-rich SEI film formed by the desolvated electrolyte on the Li metal anode and promoted uniform Li^+ ion flux deposition (Fig. 9e and f). The strategy of COF-based separators to desolvate electrolytes is promising to realize high energy density and long cycle life lithium metal batteries.

In addition to the hydrogen bonds between certain groups and the electrolyte, some emerging porous materials can also be effectively desolventized by nanochannels.[138] He *et al.*[139] found that the neutral pores of COFs are easily modified by the electrolyte solvent component groups. The Li–O bond length of the solvent increased after modification, which contributed to the breakage and achieved the desolvation of Li^+ (Fig. 9g–i). Benefiting from the aligned nanochannels, the desolvation energy of $Li(EC)^{4+}$ within the COF channel (21.67 kJ mol^{-1}) was much lower than the solvent dissociation energy (45.27 kJ mol^{-1}) in the pure electrolyte according to the theoretical calculation. The functional separator with COFs exhibited a high ionic conductivity, which was up to 8 times that of the conventional separators (Fig. 9j). The construction of functional separators to desolvate Li^+ in advance can effectively increase lithium salt concentration and inhibit lithium dendrite nucleation.

4.2 Artificial SEI

The formation of SEI films is inevitable and the inherent homogeneity of SEI plays a critical role in Li dendrite

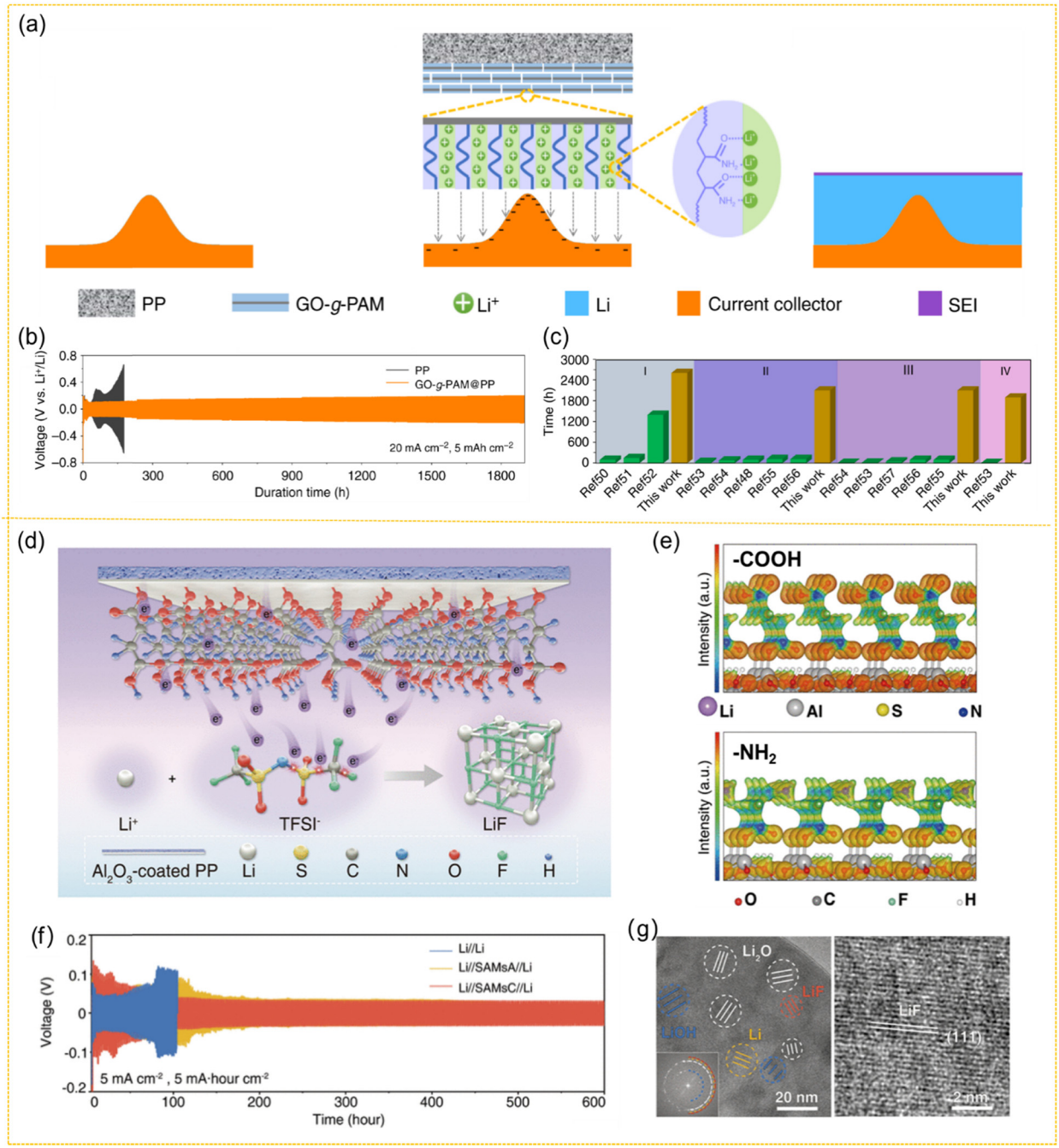

Fig. 8 The functional separator with polar groups. (a) Schematic of Li deposition behavior with a GO-*g*-PAM@PP separator. (b) Cycling performance of Li//Li symmetrical batteries with different separators. (c) Comparison of the cycle life of symmetric Li|Li cells with different separators. Reproduced with permission from ref. 132. Copyright 2019, Nature. (d) Schematic of the interaction between polar groups in self-assembled monolayers (SAMs) and LiTFSI. (e) Electrostatic potential of Al_2O_3-$OOC(CH_2)_2COOH$ and Al_2O_3-$OOC(CH_2)_2NH_2$. (f) Cycling performance of Li//Li symmetrical batteries with different separators. (g) Cryo-STEM image of the Li/Al_2O_3-$OOC(CH_2)_2COOH$ interface. Reproduced with permission from ref. 134. Copyright 2022, Science Note: electrolyte is LiTFSI (1.0 M) in DOL and DME (DOL/DME, 1 : 1 by volume) with 1 wt% $LiNO_3$.

suppression. In addition, Li whiskers are preferentially deposited in the fragile SEI film under the stress-driven SEI film. Therefore, constructing a dense and uniform SEI film can protect the Li metal from electrolyte attack and regulate the ion deposition direction.[140] Artificial SEI films not only improve interfacial stability and suppress volume changes, but also enhance surface lithophilicity and Li^+ flux redistribution. Moreover, it endows LMAs with uniform and dense electrode/electrolyte interfaces, which can redistribute Li^+ flux and tolerate lithium dendrite growth.[141,142] Inorganic substances (lithium-containing compounds) with good mechanical properties and conductivity accompanied with

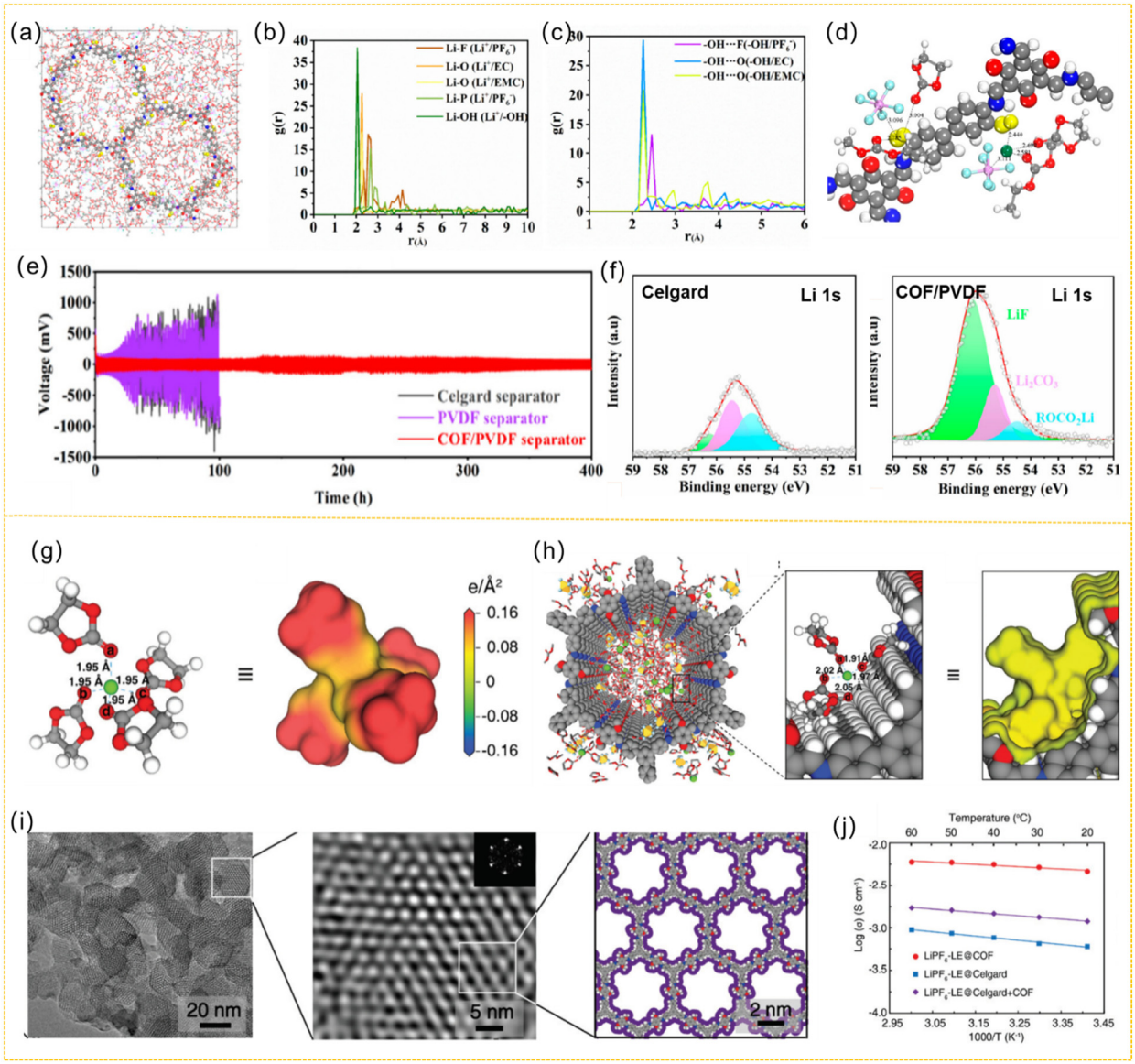

Fig. 9 The functional separator promotes the desolvation of Li^+ *via* desolvation interfaces. (a) MD models of COFs. The radial distribution functions (RDFs) between the electrolyte and Li^+ (b) and hydrogen bond (c). (d) MD snapshot of a Li^+ solvated shell in a COF channel. (e) Cycling performance of Li–Li symmetrical batteries with different separators. (f) The XPS Li 1s spectra of the Li metal surface after cycling. Reproduced with permission from ref. 137. Copyright 2022, American Chemical Society. (g) Bond lengths and charge distribution of free $Li(EC)_4^+$. (h) Bond lengths and charge distribution of free $Li(EC)_4^+$ in the COFs channel. (i) The channel structure of COFs. (j) Ionic conductivities of different samples. Reproduced with permission from ref. 139. Copyright 2020, The Royal Society of Chemistry.

an organic material (polymer) with outstanding resilience and adhesion are always used to design functional artificial SEI films.[143–145]

The LiF is considered to be a favorable component of SEI films to regulate the morphology of Li^+ deposition.[146] Kang and co-workers[147] reported a high-dielectric SEI (LiF@PVDF), which could effectively redistribute Li^+ ion flux and release locally accumulated charge density and suppress lithium protrusions, as shown in Fig. 10a. Moreover, the simulation of an interface overpotential also indicates that the LiF@PVDF SEI film decreased the overpotential of the interface medium during Li^+ deposition, which could change the Li^+ deposition morphology and alleviate the dendrite nucleation growth (Fig. 10b). The morphology of lithium can be reversibly deposited, which was confirmed by the cross-sectional SEM images. The artificial SEI film could induce the homogeneous and reversible electrochemical Li plating/stripping even at a large utilization level of 10 mA h cm^{-2} (Fig. 10c and d).

In situ construction of organic artificial SEI film on the surface of lithium metal is able to stabilize the continuous reaction in the electrolyte.[148] As shown in Fig. 10e, Tao and co-workers *in situ* constructed a carbon-based nanostructured hybrid (denoted as ECH) artificial SEI film on lithium metal by electrolysis of 1,2-dimethoxyethane (DME) solvent to direct

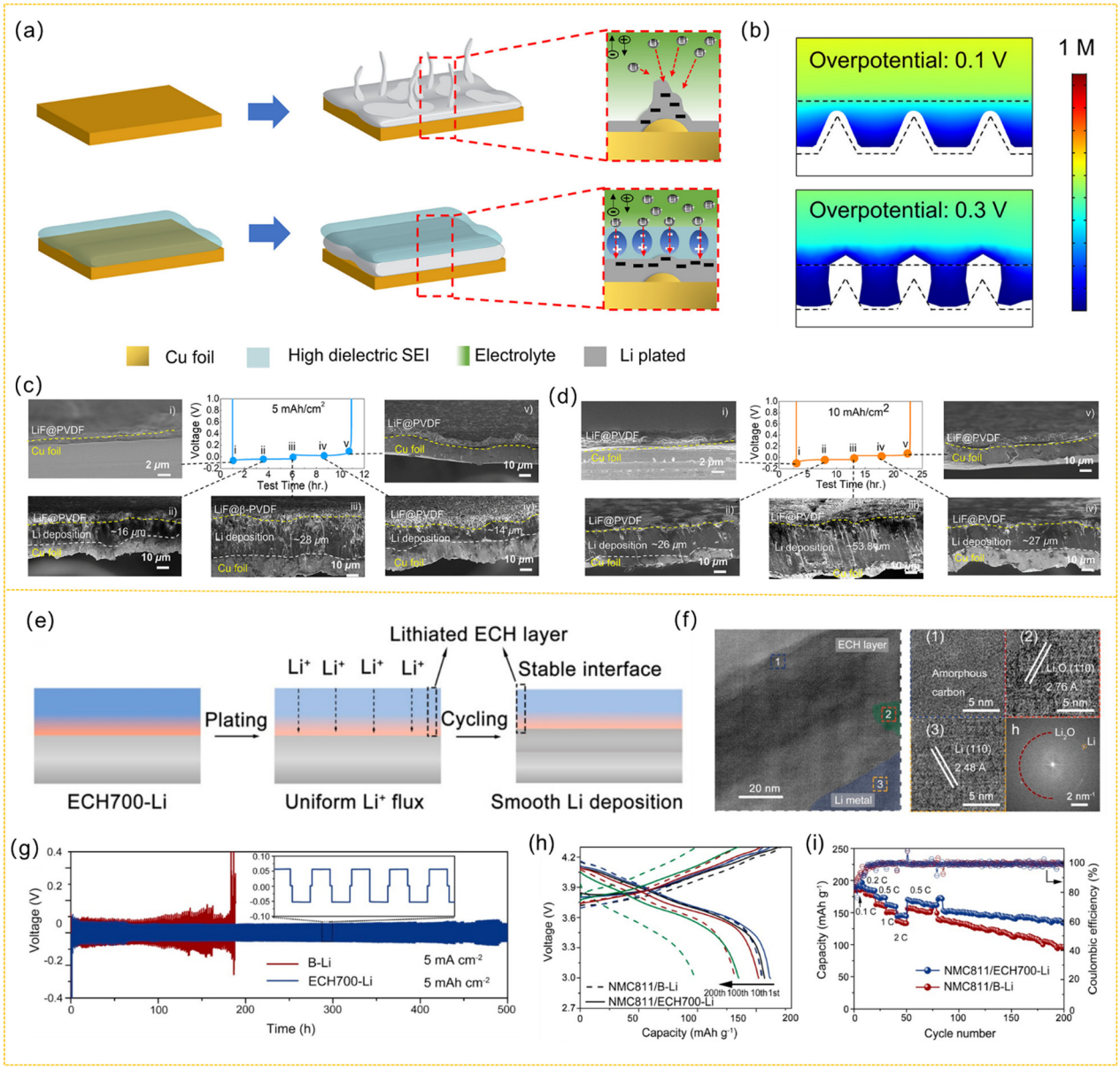

Fig. 10 The inorganic and organic artificial SEI films stabilized the Li metal anode. (a) Schematic illustrations of Li dendrites growth with or without the artificial SEI film. (b) The simulation of lithium concentration gradients on the artificial SEI film (0.1 V) and the bare metal (0.3 V). Li plating and stripping behaviors of artificial SEI film at a capacity loading of 5 mA h cm^{-2} (c) and 10 mA h cm^{-2} (d). Reproduced with permission from ref. 147. Copyright 2021, American Chemical Society. (e) Li plating/stripping behaviors for the organic SEI film (ECH700-Li) anode. (f) Cryo-TEM images of ECH700-Li. (g) Cycling performance of Li–Li symmetrical cells with or without the ECH700-Li. (h and i) Charge–discharge curves and rate capability of NMC811//Li with or without ECH700-Li full cells. Reproduced with permission from ref. 149. Copyright 2022, American Chemical Society.

the deposition of Li^+.[149] The components of ECH were investigated by Cryo-TEM (Fig. 10f). ECH contained lithium oxide and polymer layers dominated by the C–O group (inner) and amorphous carbon component (outer), which could seal the Li metal surface and enhance mechanical strength and lithium ion conductivity. In addition, the strong Li^+ affinity of the C–O bond meant that the ECH layer could be lithiated after cycling, resulting in a continuous Li^+ adsorption effect and dendrite-free lithium deposition (Fig. 10g). Furthermore, the full cell matched with NMC811 with excellent electrochemical performance also confirmed the potential of designing artificial SEI film to stabilize LMAs (Fig. 10h and i).

4.3 Solid electrolyte

The electrochemical performance with an emphasis on energy density and safety is becoming increasingly important as the demand for secondary batteries continues to increase. Lithium metal batteries with solid state electrolytes are promising as alternative energy storage technology, which can alleviate Li dendrite growth and effectively avoid liquid electrolyte fires.[150–152] Moreover,

solid state electrolyte addresses the problem of electrode/electrolyte interfaces formed by liquid electrolyte during charging and discharging by regulating lithium ion transport, which greatly improves the cycle life of lithium batteries.[153]

Despite the promising application of solid electrolytes in Li–metal batteries, the contact problem between solid electrolyte and Li–metal interface hinders the practical development of solid Li–metal batteries.[154] Bruce[114] deposited amorphous

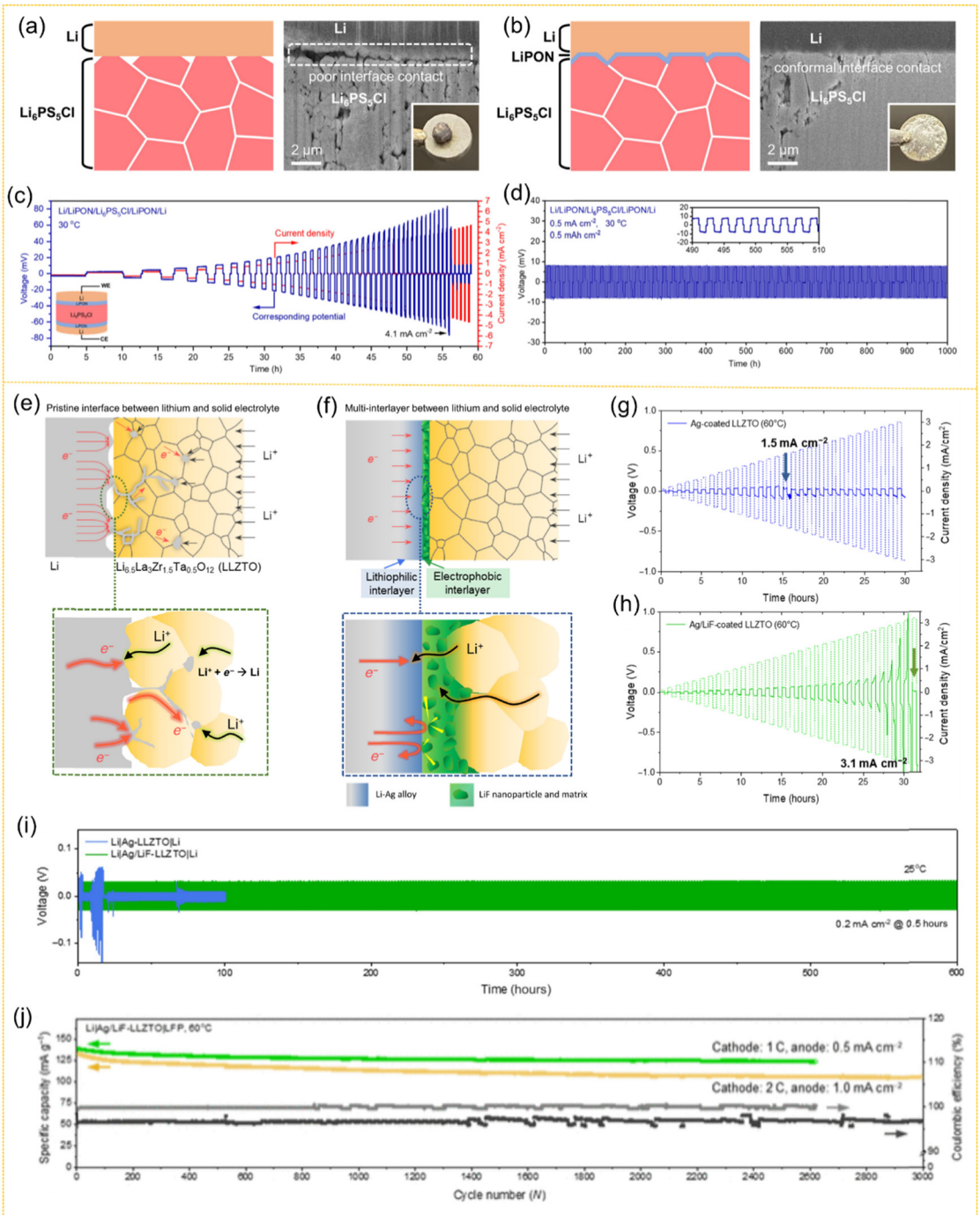

Fig. 11 Solid state electrolyte for suppressing Li dendrite growth. Schematic of the interfacial contact between Li metal and Li_6PS_5Cl (a) and LiPON@Li_6PS_5Cl (b). (c) The critical current density of Li/LiPON@Li_6PS_5Cl@LiPON/Li symmetric cells. (d) Galvanostatic cycling performance of Li/LiPON@Li_6PS_5Cl@LiPON/Li symmetric cells. Reproduced with permission from ref. 114. Copyright 2020, The Royal Society of Chemistry. Schematic illustrations of the Li metal/solid electrolyte interface. (e) Conventional interface with Li dendrite formation. (f) Lithiophilic and electron-blocking interlayers suppress Li dendrite growth. (g and h) The critical current density of Ag-coated and Ag/LiF-coated LLZTO solid electrolyte. (i) Galvanostatic cycling stability of lithium symmetric cells at 0.2 mA cm^{-2} for 0.5 hours. (j) Cycle performance of Li//NCM111 cells with Ag/LiF-coated LLZTO at 0.5 C (~0.25 mA cm^{-2}). Reproduced with permission from ref. 155. Copyright 2022, Science.

LiPON on the solid-state electrolytes (SSEs) Li_6PS_5Cl, which improved the interfacial contact with the Li metal anode and stabilized its interface. The conformal interfacial contact was formed by LiPON and Li_6PS_5Cl, which could promote the migration of lithium ions at the interface and improved the ionic conductivity (Fig. 11a and b). Moreover, the LiPON interlayer with electronically insulating properties could further alleviate the side reactions. LiPON-coated Li_6PS_5Cl symmetric cells were capable of cycling for more than 1000 h with a polarization voltage of 7.9 mV at 0.5 mA cm^{-2}, and the critical current density was up to 4.1 mA cm^{-2} (Fig. 11c and d).

Solid-state electrolytes should not only regulate ion diffusion but also focus on electron leakage. Kang and co-workers[155] demonstrated a conventional LLZTO modified by an Ag/LiF multilayer to enhance the electrochemical performance of LMAs. The lithiophilic silver layer improved the wettability of

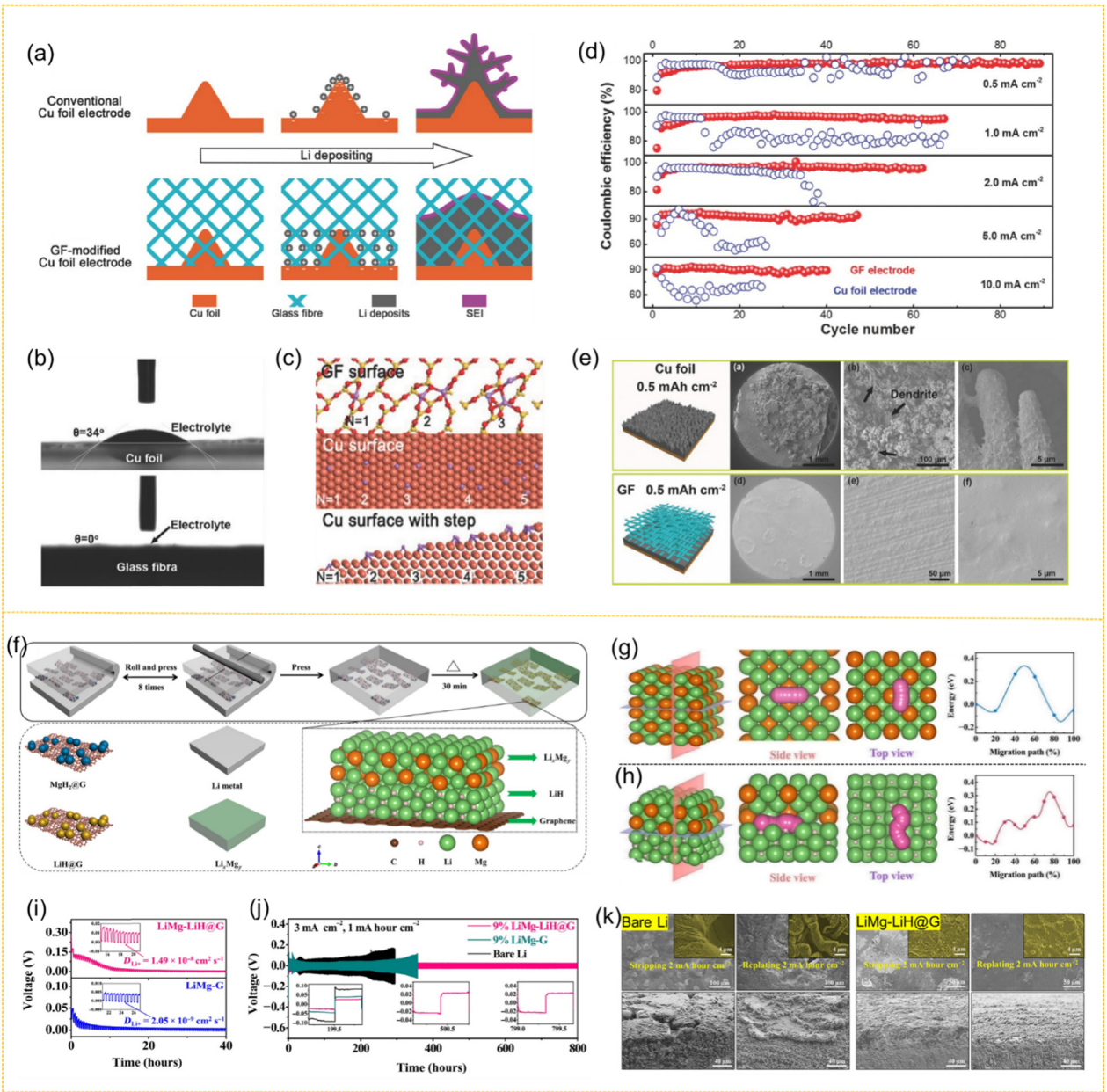

Fig. 12 Structure anode for suppressing Li dendrite growth. (a) Schematic diagrams of Li deposition on the conventional Cu and GF (glass fiber)-modified Cu foil. (b) Electrolyte wettability of Cu and GF-modified Cu foil. (c) Different numbers (*N*) of Li atoms with different surfaces. (d) Coulombic efficiency of Li deposition on bare Cu and GF-modified Cu foil at 0.5 to 10 mA cm^{-2}. (e) The Li deposits morphologies on Cu and GF-modified Cu substrates. Reproduced with permission from ref. 130. Copyright 2016, Willey. (f) Schematic illustration of the design of the LiMg-LiH@G electrode. The diffusion pathway and calculated energy of Li transport the interface of (g) Li_3Mg_7 (001)/Li_3Mg_7 (001) and (h) LiH (001)/Li_3Mg_7 (001). note: orange balls (Mg atoms), green balls (Li atoms) and pink balls (adsorbed Li atoms). (i) GITT curves and Li^+ diffusion coefficient of different samples. (j) The cycling performance of symmetric cells of different samples. (k) SEM images of bare Li and the LiMg-LiH@G anode after stripping and replating 2 mA h cm^{-2} of Li. Reproduced with permission from ref. 158. Copyright 2022, Science.

the Li metal/LLZTO interface, which decreased the interfacial resistance to less than 13.4 Ohm cm^{-2}. Moreover, the unique electron-blocking LiF layer mitigated electron conduction through the solid-state electrolyte even at high temperatures while maintaining sufficiently high lithium-ion conductivity (Fig. 11e and f). Therefore, the Li//Li symmetric cells with an Ag/LiF multilayer exhibited a record critical current density of 3.1 mA cm^{-2} at 60 °C and a stable cycling performance (Fig. 11g–i). Notably, the hybrid full cells made from LFP cathodes exhibited excellent performance at high current densities (2 C; ~1.0 mA cm^{-2}), the highest performance reported to date (Fig. 11j).

In conclusion, designing novel SSEs that can regulate lithium and electron transport is promising to break through the bottleneck of high energy density LMAs.

4.4 Structured anode

As a Li host electrode, the Li metal anode plays a critical role in normalizing Li^+ flux and stabilizing the SEI layer to tolerate the volume change during Li plating/stripping.[156] Moreover, the mechanical stability of the SEI film and battery operating life are also affected by the properties of the anode. Therefore, an ideal Li matrix should have the advantage of good physical and chemical stability and mechanical stability to alleviate the volume change and homogeneous the Li^+ plating/stripping behavior.[157]

Enhancing the chemical affinity of Li^+ with the Li matrix can improve the stability of the lithium metal anode. Zhang[130] designed 3D glass fiber (GF) cloths with polar groups (Si–O, O–H, O–B) to increase the conductivity to suppress the Li dendrite growth (Fig. 12a). The GF layer improved the affinity between the Li^+ and the Li matrix and exhibited a nanoscale interfacial interaction due to the elevated binding energy verified by the calculation (Fig. 12b and c). Moreover, the electrochemical performance was also evaluated by the Li//Cu asymmetric cells. As shown in Fig. 12d, the GF electrode displayed a high Columbic efficiency and cyclic stability compared with the Cu foil electrode. Furthermore, the Li deposition morphology was determined using SEM, as shown in Fig. 12e. And the uniform morphology was obtained *via* a GF electrode due to the homogeneous distribution of Li ions driven by the thermodynamics of electroplating.

Li metal anode alloying is an effective strategy to improve lithium affinity compared to a Li matrix with chemical interactions. Yu and co-workers[158] constructed a three-dimensional (3D) lithium metal anode (LiMg-LiH@G) consisting of a solid-solution LiMg alloy and graphene loaded with LiH nanoparticles to provide uniform nucleation sites to alleviate Li dendrite nucleation (Fig. 12f). The Li^+ transport behaviors were confirmed by theoretical calculation and experimental data (Fig. 12g and h). The uniformly constructed LiH and LiMg alloy interface formed a large amount of built-in electric field, which effectively facilitated the transfer of Li^+ from the LiH surface with the high lithium ion conductivity to the LiMg alloy surface, which was favorable for lithium deposition. As a result, the Li^+ diffusion coefficient of LiMg-LiH@G was 10 times higher than that of the LiMg-G electrode, promoting rapid Li^+ transport and stable electrochemical performance (Fig. 12i–k).

Mitigating the inherent problems of LMAs by constructing a structured anode can provide a large number of nucleophilic sites and homogenize the Li^+ flux, which provides a promising strategy for the development of dendrite-free lithium metal anodes with high energy density.

5. Conclusions and perspective

In summary, the development of high energy density LMAs is hampered by the uncontrolled Li dendrite growth and unstable SEI film caused by the disordered ion transport. Herein, the inherent relationships between Li dendrites, SEI films and Li^+ ion transport are investigated in depth to gain the optimum measures of enhancing the electrochemical performance of LMAs. Moreover, the measures of regulating Li^+ flux such as functional separators, artificial SEI films, solid-state electrolytes and structured anodes are summarized to suppress the Li dendrite growth and construct robust SEI films. A detailed summary of the issues and opportunities improves the safety and commercialization of lithium metal batteries.

Although the instability (Li dendrites and unstable SEI films) of lithium metal anodes has been improved, several critical issues still need further in-depth study and need to be addressed. The mechanism and relationships of Li^+ ion transport inside the cell (across the separator, diffusion in the electrolyte and SEI film) are ambiguous. Comprehensive and integrated approaches can alleviate the above problems. The following measures are recommended for designing excellent electrochemical performance and safety of lithium metal batteries.

(1) Comprehensive study of Li^+ ion transport mechanisms. Ion transport pathways and mechanisms play a critical role in the electrochemical performance of LMAs. However, the relationship between lithium-ion transport mechanisms and electrochemical performance is indistinct. Therefore, a theoretical model is constructed based on the experimental results to simulate the transport behavior of Li^+ ions inside the battery. And the theoretical basis for the modification of lithium metal anodes can be obtained by the Li^+ ions transport activation energy through different regions.

(2) Advanced characterization and analysis of lithium dendrites and SEI films. The electrochemical reaction inside the cell is a transient and dynamic process that should be researched by high-end *in situ* techniques to precisely study in depth. *In situ* optical microscopy, *in situ* scanning electronic microscopy (SEM), *in situ* transmission electron microscopy (TEM), and *in situ* cryo-scanning TEM (cro-TEM) with wide spatial resolutions can be used to investigate the morphology of Li dendrite and SEI films. The components and structure evolution of Li dendrites and SEI films can be analyzed by *in situ* X-ray-based techniques, *in situ* Ramman, *in situ* nuclear magnetic resonance spectroscopy (NMR) and secondary ion mass spectrometry (SIMS). In particular, magnetic resonance

imaging (MRI) and titration gas chromatography (TGC) combined with battery electrochemical curves quantitatively distinguish the active lithium lost in lithium dendrites and SEI films to find the culprits of battery performance degradation.

(3) Constructing interaction mechanisms. Disordered ion diffusion can trigger dendrite nucleation and growth while generating unsatisfactory SEI films. Conversely, lithium dendrites and SEI films can impede the homogeneous transport of Li^+ ions, exacerbating the consumption of active lithium and deteriorating the electrochemical performance. Therefore, the interaction mechanisms between cell performance (capacity, rate and cycling performance, polarization), lithium-ion transport (ionic conductivity and ion transference number) and lithium dendrites and SEI films (morphology and component evolution) should be constructed. Moreover, experimental data and theoretical simulations are used to speculate the internal chemical environment changes of the batteries to provide a scientific basis for battery performance improvement.

(4) Establish battery performance evaluation standards. In addition to Li^+ ion transport, electrochemical performance is influenced by many other factors. The cutoff voltage, electrode loading and thickness, electrolyte type and amount have important effects on the Coulomb efficiency, capacity and operating life of the cell. The establishment of a battery performance evaluation system can reduce the influence of objective factors and improve the accuracy of studying the microscopic changes internal to the battery.

Conflicts of interest

There are no conflicts to declare.

Acknowledgements

This work was supported by the National Natural Science Foundation of China (62075002), the Beijing Nova Program (Z201100006820112, 20220484234) and the Natural Science Foundation of Beijing Municipality (2212001).

References

1 W. H. Zuo, M. Z. Luo, X. S. Liu, J. Wu, H. D. Liu, J. Li, M. Winter, R. Fu, W. L. Yang and Y. Yang, *Energy Environ. Sci.*, 2020, **13**, 4450–4497.
2 A. Banerjee, X. F. Wang, C. C. Fang, E. Wu and Y. S. Meng, *Chem. Rev.*, 2020, **120**, 6878–6933.
3 X. R. Li, Y. Tian, L. Shen, Z. B. Qu, T. Q. Ma, F. Sun, X. Y. Liu, C. Zhang, J. Q. Shen, X. Y. Li, L. N. Gao, S. X. Xiao, T. F. Liu, Y. Liu and Y. F. Lu, *Adv. Funct. Mater.*, 2021, **31**, 2009718.
4 X. R. Li, M. M. Lv, Y. Tian, L. Gao, T. F. Liu, Q. H. Zhou, Y. F. Xu, L. Shen, W. Y. Shi, X. Y. Li, Y. F. Lu, X. Y. Liu and S. X. Xiao, *Nano Energy*, 2021, **87**, 106214.
5 C. Zhang, X. Li, H. Wu, J. Xu, Z. Qu, F. Sun, Y. Tian, F. Li, L. Shen and Y. Lu, *ACS Appl. Energy Mater.*, 2022, **5**, 5519.
6 Q. Zhao, R. Wang, X. Hu, Y. Wang, G. Lu, Z. Yang, Q. Liu, X. Yang, F. Pan and C. Xu, *Adv. Sci.*, 2022, **9**, e2102215.
7 M. Yang, S. Zybin, T. Das, B. Merinov, W. Goddard, E. Mok, H. Hah, H. Han, Y. Choi and S. Kim, *Adv. Energy Mater.*, 2022, **13**, 2202949.
8 J. Steiger, D. Kramer and R. Mönig, *Electrochim. Acta*, 2014, **136**, 529–536.
9 J. Tan, J. Matz, P. Dong, J. Shen and M. Ye, *Adv. Energy Mater.*, 2021, **11**, 2100046.
10 X. Y. Shan, Y. Zhong, L. J. Zhang, Y. Q. Zhang, X. H. Xia, X. L. Wang and J. P. Tu, *J. Phys. Chem. C*, 2021, **125**, 19060.
11 X. B. Cheng, C. Yan, X. Q. Zhang, H. Liu and Q. Zhang, *ACS Energy Lett.*, 2018, **3**, 1564–1570.
12 G. X. Lu, J. W. Nai, D. Y. Luan, X. Y. Tao and X. W. Lou, *Sci. Adv.*, 2023, **9**, eadf1550.
13 J. Y. Li, Y. Z. Zhang, R. Shang, C. Cheng, Y. Cheng, J. X. Xing, Z. Z. Wei and Y. Zhao, *Energy Storage Mater.*, 2021, **43**, 143–157.
14 Y. D. Wang, J. C. Liang, X. M. Song and Z. Jin, *Energy Storage Mater.*, 2023, **54**, 732–775.
15 J. Wang, L. G. Li, H. M. Hu, H. F. Hu, Q. H. Guan, M. Huang, L. J. Jia, H. Adenusi, K. Tian, J. Zhang, S. Passerini and H. Z. Lin, *ACS Nano*, 2022, **16**, 17729–17760.
16 Y. Cao, M. D. Wang, H. J. Wang, C. Y. Han, F. S. Pan and J. Sun, *Adv. Energy Mater.*, 2022, **12**, 2200057.
17 X. B. Cheng, C. Z. Zhao, Y. X. Yao, H. Liu and Q. Zhang, *Chem*, 2019, **5**, 74–96.
18 J. Um and S. Yu, *Adv. Energy Mater.*, 2020, **11**, 2003004.
19 S. Lv, T. Verhallen, A. Vasileiadis, F. Ooms, Y. Xu, Z. Li, Z. Li and M. Wagemaker, *Nat. Commun.*, 2018, **9**, 2152.
20 Q. Cheng, L. Wei, Z. Liu, N. Ni, Z. Sang, B. Zhu, W. H. Xu, M. J. Chen, Y. P. Miao, L. Q. Chen, W. Min and Y. Yang, *Nat. Commun.*, 2018, **9**, 2942.
21 S. H. Yu, X. Huang, J. D. Brock and H. D. Abruna, *J. Am. Chem. Soc.*, 2019, **141**, 8441–8449.
22 Y. He, X. D. Ren, Y. B. Xu, M. H. Engelhard, X. L. Li, J. Xiao, J. Liu, J. G. Zhang, W. Xu and C. M. Wang, *Nat. Nanotechnol.*, 2019, **14**, 1042–1047.
23 J. Steiger, D. Kramer and R. Mönig, *J. Power Sources*, 2014, **261**, 112–119.
24 K. J. Harry, D. T. Hallinan, D. Y. Parkinson, A. A. MacDowell and N. P. Balsara, *Nat. Mater.*, 2014, **13**, 69–73.
25 E. Peled, *J. Electrochem. Soc.*, 1979, **126**, 2047.
26 M. Nazri, *J. Electrochem. Soc.*, 1984, **132**, 1385.
27 D. Aurbach, M. L. Daroux, P. W. Faguy and E. Yeager, *J. Electrochem. Soc.*, 1987, **134**, 1611.
28 J. Christensen and J. Newman, *J. Electrochem. Soc.*, 2004, **151**, A1977.
29 K. Edström, M. Herstedt and D. P. Abraham, *J. Power Sources*, 2006, **153**, 380–384.
30 Y. Z. Li, Y. B. Li, A. Pei, K. Yan, Y. M. Sun, C. L. Wu, L. M. Joubert, R. Chin, A. L. Kou, Y. Yu, J. Perrino, B. Butz, S. Chu and Y. Cui, *Science*, 2017, **358**, 506–510.
31 X. Cao, X. D. Ren, L. F. Zou, M. H. Engelhard, W. Huang, H. S. Wang, B. E. Matthews, H. Lee, C. J. Niu, B. W. Arey,

Y. Cui, C. M. Wang, J. Xiao, J. Liu, W. Xu and J. G. Zhang, *Nat. Energy*, 2019, **4**, 796–805.
32 S. Jurng, Z. Brown, J. Kim and B. Lucht, *Energy Environ. Sci.*, 2018, **11**, 2600–2608.
33 Y. Z. Li, W. Huang, Y. B. Li, A. Pei, D. T. Boyle and Y. Cui, *Joule*, 2018, **2**, 2167–2177.
34 S. J. Park, J. Y. Hwang, C. S. Yoon, H. G. Jung and Y. K. Sun, *ACS Appl. Mater. Interfaces*, 2018, **10**, 17985–17993.
35 E. Peled and S. Menkin, *J. Electrochem. Soc.*, 2017, **164**, A1703.
36 S. Q. Shi, P. Lu, Z. Y. Liu, Y. Qi, L. G. Hector, H. Li and S. Harris, *J. Am. Chem. Soc.*, 2012, **134**, 15476–15487.
37 L. N. Wang, A. Menakath, F. D. Han, Y. Wang, P. Y. Zavalij, K. J. Gaskell, O. Borodin, D. Iuga, S. P. Brown, C. S. Wang, K. Xu and B. Eichhorn, *Nat. Chem.*, 2019, **11**, 789–796.
38 J. Goodenough and Y. Kim, *Chem. Mater.*, 2009, **22**, 587–603.
39 X. B. Cheng, R. Zhang, C. Z. Zhao and Q. Zhang, *Chem. Rev.*, 2017, **117**, 10403–10473.
40 S. K. Heiskanen, J. Kim and B. L. Lucht, *Joule*, 2019, **3**, 2322–2333.
41 S. T. Hong, J. S. Kim, S. J. Lim and W. Y. Yoon, *Electrochim. Acta*, 2004, **50**, 535–539.
42 D. Aurbach, Y. Talyosef, B. Markovsky, E. Markevich, E. Zinigrad, L. Asraf, J. Gnanaraj and H. Kim, *Electrochim. Acta*, 2004, **50**, 247–254.
43 J. G. Zhang, W. Xu, J. Xiao, X. Cao and J. Liu, *Chem. Rev.*, 2020, **120**, 13312–13348.
44 M. B. Pinson and M. Z. Bazant, *J. Electrochem. Soc.*, 2013, **160**, A243.
45 F. A. Soto, Y. G. Ma, J. Martinez de la Hoz, J. M. Seminario and P. B. Balbuena, *Chem. Mater.*, 2015, **27**, 7990–8000.
46 J. F. Ding, R. Xu, X. X. Ma, Y. X. Xiao, Y. Yao, C. Yan and J. Q. Huang, *Angew. Chem., Int. Ed.*, 2022, **61**, e202115602.
47 A. Groß and S. Sakong, *Curr. Opin. Electrochem.*, 2019, **14**, 1–6.
48 S. Malmgren, K. Ciosek, M. Hahlin, T. Gustafsson, M. Gorgoi, H. Rensmo and K. Edström, *Electrochim. Acta*, 2013, **97**, 23–32.
49 C. Yan, R. Xu, Y. Xiao, J. F. Ding, L. Xu, B. Q. Li and J. Q. Huang, *Adv. Funct. Mater.*, 2020, **30**, 1909887.
50 M. Winter and R. J. Brodd, *Chem. Rev.*, 2004, **104**, 4245–4270.
51 E. Peled, D. Golodnitsky and G. Ardel, *J. Electrochem. Soc.*, 1997, **144**, L208.
52 D. Aurbach, *J. Power Sources*, 2000, **89**, 206–218.
53 P. Lu and S. J. Harris, *Electrochem. Commun.*, 2011, **13**, 1035–1037.
54 D. Aurbach, E. Zinigrad, Y. Cohen and H. Teller, *Solid State Ionics*, 2002, **148**, 405–416.
55 W. Liu, J. X. Li, W. T. Li, H. Y. Xu, C. Zhang and X. Qiu, *Nat. Commun.*, 2020, **11**, 3629.
56 P. K. Nayak, J. Grinblat, M. Levi and D. Aurbach, *J. Electrochem. Soc.*, 2015, **162**, A596.
57 Z. Peng, N. Zhao, Z. G. Zhang, H. Wan, H. Lin, M. Liu, C. Shen, H. Y. He, X. Guo, J. G. Zhang and D. Y. Wang, *Nano Energy*, 2017, **39**, 662–672.
58 X. D. Ren, Y. H. Zhang, M. H. Engelhard, Q. Y. Li, J. G. Zhang and W. Xu, *ACS Energy Lett.*, 2017, **3**, 14–19.
59 L. D. Lin, L. M. Suo, Y. S. Hu, H. Li, X. J. Huang and L. Q. Chen, *Adv. Energy Mater.*, 2021, **11**, 2003709.
60 Y. Ozhabes, D. Gunceler and T. Arias, arXiv, 2015, preprint, arXiv:1504.05799 [cond-mat.mtrl-sci].
61 Y. Qiao, H. J. Yang, Z. Chang, H. Deng, X. Li and H. S. Zhou, *Nat. Energy*, 2021, **6**, 653–662.
62 J. Langdon and A. Manthiram, *Adv. Funct. Mater.*, 2021, **31**, 2010267.
63 K. Park and J. B. Goodenough, *Adv. Energy Mater.*, 2017, **7**, 1700732.
64 Y. Ein-Eli and D. Aurbach, *J. Power Sources*, 1995, **54**, 281–288.
65 P. B. Zhai, L. X. Liu, X. K. Gu, T. S. Wang and Y. J. Gong, *Adv. Energy Mater.*, 2020, **10**, 2001257.
66 Y. Yuan, F. Wu, Y. Bai, Y. Li, G. Chen, Z. Wang and C. Wu, *Energy Storage Mater.*, 2019, **16**, 411–418.
67 Y. Y. Lu, Z. Y. Tu and L. A. Archer, *Nat. Mater.*, 2014, **13**, 961–969.
68 Y. H. Tan, G. X. Lu, J. H. Zheng, F. Zhou, M. Chen, T. Ma, L. L. Lu, Y. H. Song, Y. Guan, J. X. Wang, Z. Liang, W. S. Xu, Y. G. Zhang, X. Y. Tao and H. B. Yao, *Adv. Mater.*, 2021, **33**, e2102134.
69 F. Wang, B. Wang, J. Li, B. Wang, Y. Zhou, D. Wang, H. Liu and S. Dou, *ACS Nano*, 2021, **15**, 2197.
70 Y. Yu, G. Huang, J. Du, J. Wang, Y. Wang, Z. Wu and X. Zhang, *Energy Environ. Sci.*, 2020, **13**, 3075.
71 Z. Peng, F. H. Ren, S. S. Yang, M. Q. Wang, J. Sun, D. Y. Wang, W. Xu and J. G. Zhang, *Nano Energy*, 2019, **59**, 110–119.
72 D. Aurbach and I. Weissman, *Electrochem. Commun.*, 1999, **1**, 324–331.
73 C. C. Fang, J. X. Li, M. H. Zhang, Y. H. Zhang, F. Yang, J. Z. Lee, M. H. Lee, J. Alvarado, M. A. Schroeder, Y. Yang, B. Y. Lu, N. Williams, M. Ceja, L. Yang, M. Cai, J. Gu, K. Xu, X. F. Wang and Y. S. Meng, *Nature*, 2019, **572**, 511–515.
74 M. Zachman, Z. Tu, S. Choudhury, L. Archer and L. Kourkoutis, *Nature*, 2018, **560**, 345–349.
75 Z. Shadike, H. Lee, O. Borodin, X. Cao, X. L. Fan, X. L. Wang, R. Q. Lin, S. M. Bak, S. Ghose, K. Xu, C. S. Wang, J. Liu, J. Xiao, X. Q. Yang and E. Y. Hu, *Nat. Nanotechnol.*, 2021, **16**, 549–554.
76 H. Y. Zhang, S. L. Ju, G. L. Xia and X. B. Yu, *Sci. adv.*, 2022, **8**, eabl8245.
77 J. W. Ju, S. M. Dong, Y. Y. Cui, Y. F. Zhang, B. Tang, F. Jiang, Z. L. Cui, H. R. Zhang, X. F. Du, T. Lu, L. Huang, G. L. Cui and L. Q. Chen, *Angew. Chem., Int. Ed.*, 2021, **60**, 16487–16491.
78 M. M. Tao, Y. X. Xiang, D. H. Zhao, P. Z. Shan, Y. O. Sun and Y. Yang, *Nano Lett.*, 2022, **22**, 6775–6781.
79 Y. X. Lin, Z. Liu, K. Leung, L. Q. Chen, P. Lu and Y. Qi, *J. Power Sources*, 2016, **309**, 221–230.
80 Z. Liu, Y. Qi, Y. X. Lin, L. Chen, P. Lu and L. Q. Chen, *J. Electrochem. Soc.*, 2016, **163**, A592.
81 K. Xu, A. von Cresce and U. Lee, *Langmuir*, 2010, **26**, 11538–11543.

82 K. Xu, *J. Electrochem. Soc.*, 2007, **154**, A162.
83 E. Peled, *J. Electrochem. Soc.*, 1979, **126**, 2047.
84 X. B. Cheng, R. Zhang, C. Z. Zhao, F. Wei, J. G. Zhang and Q. Zhang, *Adv. Sci.*, 2016, **3**, 1500213.
85 D. Zheng, D. Y. Qu, X. Q. Yang, H. S. Lee and D. Y. Qu, *ACS Appl. Mater. Inter.*, 2015, **7**, 19923–19929.
86 S. Uchida and M. Ishikawa, *J. Power Sources*, 2017, **359**, 480–486.
87 C. Wan, M. Y. Hu, O. Borodin, J. F. Qian, Z. H. Qin, J. G. Zhang and J. Z. Hu, *J. Power Sources*, 2016, **307**, 231–243.
88 J. F. Qian, W. A. Henderson, W. Xu, P. Bhattacharya, M. Engelhard, O. Borodin and J. G. Zhang, *Nat. Commun.*, 2015, **6**, 6362.
89 Y. Yamada, Y. Iriyama, T. Abe and Z. Ogumi, *Langmuir*, 2009, **25**, 12766–12770.
90 H. Abe, Y. Iriyama and Z. Ogumi, *J. Electrochem. Soc.*, 2004, **151**, A1120.
91 M. R. Busche, T. Drossel, T. Leichtweiss, D. A. Weber, M. L. Falk, M. Schneider, M. Reich, H. Sommer, P. Adelhelm and J. Janek, *Nat. Chem.*, 2016, **8**, 426–434.
92 O. Borodin, G. D. Smith and P. Fan, *J. Phys. Chem. B*, 2006, **110**, 22773–22779.
93 F. Single, B. Horstmann and A. Latz, *J. Electrochem. Soc.*, 2017, **164**, E3132.
94 Y. C. Chen, C. Y. Ouyang, L. J. Song and Z. L. Sun, *J. Phys. Chem. C*, 2011, **115**, 7044–7049.
95 Q. L. Zhang, J. Pan, P. Lu, Z. Y. Liu, M. W. Verbrugge, B. W. Sheldon, Y. T. Cheng, Y. Qi and X. C. Xiao, *Nano Lett.*, 2016, **16**, 2011–2016.
96 J. N. Chazalviel, *Phys. Rev. A: At., Mol., Opt. Phys.*, 1990, **42**, 7355.
97 D. C. Lin, Y. Y. Liu and Y. Cui, *Nat. Nanotechnol.*, 2017, **12**, 194–206.
98 A. Jana and R. E. García, *Nano Energy*, 2017, **41**, 552–565.
99 W. Xu, J. L. Wang, F. Ding, X. L. Chen, E. Nasybulin, Y. H. Zhang and J. G. Zhang, *Energy Environ. Sci.*, 2014, **7**, 513–537.
100 D. R. Ely and R. E. García, *J. Electrochem. Soc.*, 2013, **160**, A662.
101 C. Ling, D. Banerjee and M. Matsui, *Electrochim. Acta*, 2012, **76**, 270–274.
102 R. L. Sacci, N. J. Dudney, K. L. More, L. R. Parent, I. Arslan, N. D. Browning and R. R. Unocic, *Chem. Commun.*, 2014, **50**, 2104–2107.
103 V. Fleury, J. N. Chazalviel, M. Rosso and B. Sapoval, *J. Electroanal. Chem. Interfacial Electrochem.*, 1990, **290**, 249.
104 V. Fleury, M. Rosso, J. N. Chazalviel and B. Sapoval, *Phys. Rev. A: At., Mol., Opt. Phys.*, 1991, **44**, 6693.
105 J. Elezgaray, C. Léger and F. Argoul, *J. Electrochem. Soc.*, 1998, **145**, 2016.
106 M. Bazant, *Phys. Rev. E: Stat. Phys., Plasmas, Fluids, Relat. Interdiscip. Top.*, 1995, **52**, 1903.
107 D. Barkey and P. Laporte, *J. Electrochem. Soc.*, 1990, **137**, 1655.
108 Z. D. Hao, Y. Wu, Q. Zhao, J. D. Tang, Q. Q. Zhang, X. X. Ke, J. B. Liu, Y. H. Jin and H. Wang, *Adv. Funct. Mater.*, 2021, **31**, 2102938.
109 Q. Zhao, R. K. Zhou, C. J. Wang, J. X. Kang, Q. Q. Zhang, J. B. Liu, Y. H. Jin, H. Wang, Z. L. Zheng and L. Guo, *Adv. Funct. Mater.*, 2022, **32**, 2112711.
110 R. R. Miao, J. Yang, Z. X. Xu, J. L. Wang, Y. Nuli and L. M. Sun, *Sci. Rep.*, 2016, **6**, 21771.
111 C. Brissot, M. Rosso, J. N. Chazalviel and S. Lascaud, *J. Electrochem. Soc.*, 1999, **146**, 4393.
112 S. Choudhury, R. Mangal, A. Agrawal and L. Archer, *Nat. Commun.*, 2015, **6**, 10101.
113 R. G. Cao, J. Z. Chen, K. S. Han, W. Xu, D. H. Mei, P. Bhattacharya, M. H. Engelhard, K. T. Mueller, J. Liu and J. G. Zhang, *Adv. Funct. Mater.*, 2016, **26**, 3059–3066.
114 J. Su, M. Pasta, Z. Y. Ning, X. W. Gao, P. G. Bruce and C. R. Grovenor, *Energy Environ. Sci.*, 2022, **15**, 3805–3814.
115 J. R. Xu, J. M. Li, Y. M. Li, M. Yang, L. Q. Chen, H. Li and F. Wu, *Adv. Mater.*, 2022, **34**, e2203281.
116 X. R. Chen, Y. X. Yao, C. Yan, R. Zhang, X. B. Cheng and Q. Zhang, *Angew. Chem., Int. Ed.*, 2020, **59**, 7743.
117 X. Wang, W. Zeng, L. Hong, W. W. Xu, H. K. Yang, F. Wang, H. G. Duan, M. Tang and H. Q. Jiang, *Nat. Energy*, 2018, **3**, 227–235.
118 C. Zhou, Q. He, Z. H. Li, J. S. Meng, X. F. Hong, Y. Li, Y. Zhao, X. Xu and L. Q. Mai, *Chem. Eng. J.*, 2020, **395**, 124979.
119 Z. Chang, H. J. Yang, A. Q. Pan, P. He and H. S. Zhou, *Nat. Commun.*, 2022, **13**, 6788.
120 Z. Liang, D. C. Lin, J. Zhao, Z. D. Lu, Y. Y. Liu, C. Liu, Y. Y. Lu, H. T. Wang, K. Yan, X. Y. Tao and Y. Cui, *Proc. Natl. Acad. Sci. U. S. A.*, 2016, **113**, 2862–2867.
121 K. Yan, Z. D. Lu, H. W. Lee, F. Xiong, P. C. Hsu, Y. Z. Li, J. Zhao, S. Chu and Y. Cui, *Nat. Energy*, 2016, **1**, 16010.
122 Y. Y. Liu, S. Z. Xiong, J. L. Wang, X. X. Jiao, S. Li, C. F. Zhang, Z. X. Song and J. X. Song, *Energy Storage Mater.*, 2019, **19**, 24–30.
123 Y. Cao, H. Wu, G. Li, C. Liu, L. Cao, Y. M. Zhang, W. Bao, H. L. Wang, Y. Yao, S. Liu, F. S. Pan, Z. Y. Jiang and J. Sun, *Nano Lett.*, 2021, **21**, 2997–3006.
124 Z. P. Zhu, D. Y. Wang, Y. Tian and L. Jiang, *J. Am. Chem. Soc.*, 2019, **141**, 8658–8669.
125 C. Wang, J. D. Tang, L. Y. Li, J. H. Wan, Y. C. Ma, Y. H. Jin, J. B. Liu, H. Wang and Q. Q. Zhang, *Adv. Funct. Mater.*, 2022, **32**, 2204068.
126 L. H. Xie, J. D. Tang, R. N. Qin, Q. Q. Zhang, J. B. Liu, Y. H. Jin and H. Wang, *Adv. Funct. Mater.*, 2022, **33**, 2208959.
127 S. Eun Park, K. Shin, J. Hyuk Yang, B. Keun Park, S. Yeun Kim, H. Kim, M. Park and K. Jae Kim, *Chem. Eng. J.*, 2022, **445**, 136801.
128 C. Zhang, L. Shen, J. Q. Shen, F. Liu, G. Chen, R. Tao, S. X. Ma, Y. T. Peng and Y. F. Lu, *Adv. Mater.*, 2019, **31**, e1808338.
129 C. Wang, J. D. Tang, Z. Y. Chen, Y. H. Jin, J. B. Liu, H. Xu, H. Wang, X. M. He and Q. Q. Zhang, *Energy Storage Mater.*, 2022, **55**, 498–516.

130 X. b Cheng, T. z Hou, R. Zhang, H. J. Peng, C. Z. Zhao, J. Q. Huang and Q. Zhang, *Adv. Mater.*, 2016, **28**, 2888–2895.
131 Z. Liang, G. Y. Zheng, C. Liu, N. Liu, W. Y. Li, K. Yan, H. B. Yao, P. C. Hsu, S. Chu and Y. Cui, *Nano Lett.*, 2015, **15**, 2910–2916.
132 C. F. Li, S. H. Liu, C. G. Shi, G. H. Liang, Z. T. Lu, R. W. Fu and D. C. Wu, *Nat. Commun.*, 2019, **10**, 1363.
133 M. Mitsuya, *Langmuir*, 1994, **10**, 1635–1637.
134 Y. J. Liu, X. Y. Tao, Y. Wang, C. Jiang, C. Ma, Q. Sheng, G. X. Lu and X. W. Lou, *Science*, 2022, **375**, 739–745.
135 Z. Chang, H. J. Yang, Y. Qiao, X. Y. Zhu, P. He and H. S. Zhou, *Adv. Mater.*, 2022, **34**, e2201339.
136 Z. Chang, Y. Qiao, H. Deng, H. J. Yang, P. He and H. Zhou, *Joule*, 2020, **4**, 1776–1789.
137 Y. Yang, S. Y. Yao, Z. W. Liang, Y. C. Wen, Z. B. Liu, Y. W. Wu, J. Liu and M. Zhu, *ACS Energy Lett.*, 2022, **7**, 885–896.
138 Z. Chang, Y. Qiao, H. J. Yang, H. Deng, X. Y. Zhu, P. He and H. S. Zhou, *Energy Environ. Sci.*, 2020, **13**, 4122–4131.
139 L. Sheng, L. Wang, J. L. Wang, H. Xu and X. M. He, *Chem. Commun.*, 2020, **56**, 10465–10468.
140 R. Y. Deng, F. L. Chu, F. Kwofie, Z. Q. Guan, J. Chen and F. X. Wu, *Angew. Chem., Int. Ed.*, 2022, **61**, e202215866.
141 P. L. Li, X. L. Dong, C. Li, J. Y. Liu, Y. Liu, W. L. Feng, C. X. Wang, Y. G. Wang and Y. Y. Xia, *Angew. Chem., Int. Ed.*, 2019, **137**, 2115–2119.
142 B. Zhu, Y. Jin, X. Z. Hu, Q. H. Zheng, S. Zhang, Q. J. Wang and J. Zhu, *Adv. Mater.*, 2017, **29**, 1603755.
143 K. Chen, R. Pathak, A. Gurung, E. A. Adhamash, B. Bahrami, Q. Y. He, H. Qiao, A. L. Smirnova, J. J. Wu, Q. Q. Qiao and Y. Zhou, *Energy Storage Mater.*, 2019, **18**, 389–396.
144 Q. F. Yang, M. N. Cui, J. L. Hu, F. L. Chu, Y. J. Zheng, J. J. Liu and C. L. Li, *ACS Nano*, 2020, **14**, 1866–1878.
145 F. F. Liu, L. F. Wang, Z. W. Zhang, P. C. Shi, Y. Z. Feng, Y. Yao, S. F. Ye, H. Y. Wang, X. J. Wu and Y. Yu, *Adv. Funct. Mater.*, 2020, **30**, 2001607.
146 B. Zhong, J. Y. Wu, L. T. Ren, T. Y. Zhou, Z. J. Zhang, W. Liu and H. H. Zhou, *Energy Storage Mater.*, 2022, **50**, 792–801.
147 O. Tamwattana, H. Park, J. Kim, I. Hwang, G. Yoon, T. H. Hwang, Y. S. Kang, J. Park, N. Meethong and K. Kang, *ACS Energy Lett.*, 2021, **6**, 4416–4425.
148 D. D. Chen, S. Huang, L. Zhong, S. J. Wang, M. Xiao, D. M. Han and Y. Z. Meng, *Adv. Funct. Mater.*, 2019, **30**, 1907717.
149 G. X. Lu, J. W. Nai, H. D. Yuan, J. C. Wang, J. H. Zheng, Z. J. Ju, C. B. Jin, Y. Wang, T. F. Liu, Y. J. Liu and X. Y. Tao, *ACS Nano*, 2022, **16**, 9883–9893.
150 A. Manthiram, X. W. Yu and S. F. Wang, *Nat. Rev. Mater.*, 2017, **2**, 16103.
151 J. Janek and W. G. Zeier, *Nat. Energy*, 2016, **1**, 16141.
152 W. J. Zhao, J. Yi, P. He and H. S. Zhou, *Electrochem. Energy Rev.*, 2019, **2**, 574–605.
153 V. Thangadurai, S. Narayanan and D. Pinzaru, *Chem. Soc. Rev.*, 2014, **43**, 4714–4727.
154 J. Tippens, J. C. Miers, A. Afshar, J. A. Lewis, F. J. Q. Cortes, H. P. Qiao, T. S. Marchese, C. Di Leo, C. Saldana and M. T. McDowell, *ACS Energy Lett.*, 2019, **4**, 1475–1483.
155 S. Lee, K. S. Lee, S. Kim, K. Yoon, S. Han, M. H. Lee, Y. Ko, J. H. Noh, W. Kim and K. Kang, *Sci. Adv.*, 2022, **30**, eabq0153.
156 X. Q. Zhang, X. B. Cheng and Q. Zhang, *J. Energy Chem.*, 2016, **25**, 967–984.
157 I. Yang, J. H. Jeong, J. Y. Seok and S. Kim, *Adv. Energy Mater.*, 2022, **13**, 2202321.
158 H. Y. Zhang, S. L. Ju, G. L. Xia and X. B. Yu, *Sci. adv.*, 2022, **8**, eabl8245.

